DETECTION OF ATTENTION DEFICIT HYPERACTIVITY DISORDER BY USING EEG SIGNALS AND DEEP LEARNING

EFE UTKU COŞMAZ

Thesis for the Master's Program in Electrical and Electronics Engineering

Graduate School

Izmir University of Economics

Izmir

2024

DETECTION OF ATTENTION DEFICIT HYPERACTIVITY DISORDER BY USING EEG SIGNALS AND DEEP LEARNING

EFE UTKU COŞMAZ

THESIS ADVISOR: PROF. DR. AYDIN AKAN

A Master's Thesis

Submitted to

the Graduate School of Izmir University of Economics

the Department of Electrical and Electronics Engineering

Izmir

2024

ETHICAL DECLARATION

I hereby declare that I am the sole author of this thesis and that I have conducted my work in accordance with academic rules and ethical behaviour at every stage from the planning of the thesis to its defence. I confirm that I have cited all ideas, information and findings that are not specific to my study, as required by the code of ethical behaviour, and that all statements not cited are my own.

Name, Surname: Efe Utku Coşmaz

Date:12.01.2024

Signature:

ABSTRACT

DETECTION OF ATTENTION DEFICIT HYPERACTIVITY DISORDER BY
USING EEG SIGNALS AND DEEP LEARNING

Coşmaz, Efe Utku

Master's Program in Electrical and Electronics Engineering

Advisor: Prof. Dr. Aydın AKAN

January, 2024

Attention deficit hyperactivity disorder (ADHD) is a neurological disorder generally seen in children, and early diagnosis is extremely important. Electroencephalography (EEG) signals are used extensively to diagnose ADHD. In this study, resting state EEG signals from ADHD patients and healthy control subjects in the same age group were recorded at the Izmir Katip Celebi University, Department of Neurology, and analyzed. Intrinsic mode functions (IMF) were extracted by the Empirical Mode Decomposition (EMD) method. Then, short-term Fourier transform spectrograms of IMFs as well as the EEG signals were calculated and saved as colored images. Finally, the spectrogram images were classified by training two-dimensional Convolutional Neural Networks (2D-CNN) using different brain regions or the whole brain. In our simulations, almost 92% classification accuracy was achieved with the CNN structure designed in the Python environment, and 96.526% classification accuracy was achieved with the ResNet50 architecture.

ÖZET

DİKKAT EKSİKLİĞİ HİPERAKTİVİTE BOZUKLUĞUNUN EEG SİNYALLERİ VE DERİN ÖĞRENMEYLE TESPİTİ

Coşmaz**,** Efe Utku

Elektrik ve Elektronik Mühendisliği Yüksek Lisans Programı

Tez Danışmanı: Prof. Dr. Aydın AKAN

Ocak, 2024

Dikkat eksikliği hiperaktivite bozukluğu (DEHB) genelikle çocuklarda görülen, nörolojik bir hastalıktır. Bu hastalık yaşam kalitesini düşürdüğü için erken teşhis son derece önemlidir. Elektroensefalografi (EEG) bir nörogörüntüleme tekniği olup DEHB teşhisinde yoğun olarak kullanılmaktadır. Bu çalışmada aynı yaş grubundaki DEHB tanısı konmuş bireyler ve sağlıklı kontrol bireylerden dinlenme durumu EEG sinyaleri İzmir Katip Çelebi Üniversitesi, Nöroloji Kliniğinde kayıt edilmiştir. Görgül Kip Ayrışım (GKA: EMD) yöntemi ile içkin kip fonksiyonları (IMF) elde edilmiştir. Daha sonra IMF'ler ve EEG sinyallerinin kısa süreli Fourier dönüşümü yardımı ile spektrogramları hesaplanmış ve renkli imgeler olarak kaydedilmiştir. Daha sonra spektrogram imgeleri beynin farklı bölgeleri ve bütünü bir arada kullanılarak iki boyutlu Evrişimsel Sinir Ağları (2D-CNN) eğitilerek sınıflandırılmıştır. Yapılan testlerde Python ortamında tasarlanmış olan CNN yapısı ile yaklaşık %92, ResNet50 mimarisi ile % 96.526 sınıflandırma doğruluğuna ulaşılmıştır.

Anahtar Kelimeler: Elektroensefalografi (EEG), Dikkat Eksikliği Hiperaktivite Bozukluğu (DEHB), Görgül Kip Ayrışımı (GKA), Derin Öğrenme, Spektrogram.

To my family...

ACKNOWLEDGEMENTS

I would like to express my deepest thanksgiving to my supervisor, Prof. Dr. Aydın Akan. Also, I would like to sincerely thank Asst. Prof. Özlem Karabiber Cura. I feel very lucky to be their student.

I would also like to thank my father Mehmet Coşmaz, for supporting me in everything.

TABLE OF CONTENTS

LIST OF TABLES

LIST OF FIGURES

LIST OF ABBREVIATIONS

EMD: Empirical Mode Decomposition

IMF: Intrinsic Mode Function

STFT: Short Time Fourier Transform

ADHD: Attention Deficit Hyperactivity Disorder

EEG: Electroencephalography

CNN: Convolutional Neural Network

DL: Deep Learning

FT: Fourier Transform

GPU: Graphics Processing Unit

CPU: Central Process Unit

ANN: Artificial Neural Network

ACC: Accuracy

SEN: Sensitivity

SPE: Specificity

FDR: False Discovery Rate

PRE: Precision

MEMD: Multivariate Empirical Mode Decomposition

ITD: Intrinsic Time-scale Decomposition

EEMD: Ensemble Empirical Mode Decomposition

CNS: Central Nervous Syste

IDE: Integrated Development Environment

CHAPTER 1: INTRODUCTION

Attention deficit hyperactivity disorder (ADHD) is a neurodevelopmental problem generally seen in very young children and during childhood. It can affect children as young as four years old (Andreasen et al., 2023). Children affected by ADHD have deficiencies in their emotional, cognitive and social development, entailing difficulties in their future education, their academic work and social life (Nazari et al., 2023). They have difficulty in performing daily activities and they suffer from forgetfulness as well concerning their behavior in their social environment, failures at work or school are common (Alberola-López et al., 2023). Five percent of the children in the world have ADHD (Li et al., 2021). In order to be diagnosed with ADHD, the child must be under 12 years old. In addition, symptoms of the disease must have lasted for about 6 months.

One way to diagnose ADHD are brain signals. Brain signaling studies can be used as a diagnosis based on quantitative data (Cura, Atli and Akan, 2023). The electroencephalography (EEG) signal provides information on the changes of electrical potential in the human brain. Information is obtained through signals coming from electrodes placed on the patient's scalp. Apart from psychological observation and interviews, there are different technical approaches to the diagnosis of ADHD, including functional neuroimaging techniques, magnetic resonance imaging, and neurophysiological signal analysis (Bakhtyari and Mirzaei, 2022). Trying to diagnose ADHD using only psychological observations or clinical interviews provides low reliability (Cura, Atli and Akan, 2023). Functional neuroimaging and magnetic resonance imaging techniques are expensive. Both methods are time-consuming. The above stated method of using electroencephalogram (EEG) signals to detect brain activity is effective and low-cost. Therefore, the EEG is widely used (Jahed et al., 2022).

In this study, intrinsic mode functions (IMFs) of EEG signals were obtained using empirical mode decomposition (EMD). The first 5 IMFs were used in this study. These obtained IMFs were converted into RGB images using the spectrogram method. Then, these images were classified with convolutional neural network (CNN) with the help of deep learning method. Three different architectures were used in this classification process. Two of these architectures were designed in Python programming language.

Spider was used as the integrated development environment (IDE). The last CNN architecture used is the ResNet50 architecture in the Matlab environment.

CHAPTER 2: BACKGROUND

This chapter includes information on those processes of the brain, which are the primary source of neurological diseases. In addition, the chapter informs about the epidemiology and clinical history of ADHD and includes a review of the pertinent literature. Finally, the EEG recording method will be discussed, which is widely used in the clinical and the academic field, and on which this study focuses.

2.1 The Structure and Function of the Human Brain

The brain, which weighs approximately 1.5 kg in an adult human, is the most important part of the Central Nervous System (CNS). There are, on average, 84 billion neurons in the brain and it consists of trillions of glials. Although it constitutes only 2% of the total body mass, 20% of the total energy is consumed by the brain. The brain controls the limbs based on the sensory information it receives from the spinal cord and nerves (Lewis et al., 2023)

The brain has three main parts: the forebrain, midbrain, and hindbrain. The forebrain performs tasks such as problem-solving and information processing. The hindbrain has functions such as regulating autonomic functions, directing sensory information, and maintaining balance. The midbrain has functions such as organizing and processing auditory and visual information.

The brain is an extremely complex organ. The working areas are often dispersed across multiple regions. The parts of the brain are as in Figure 1.
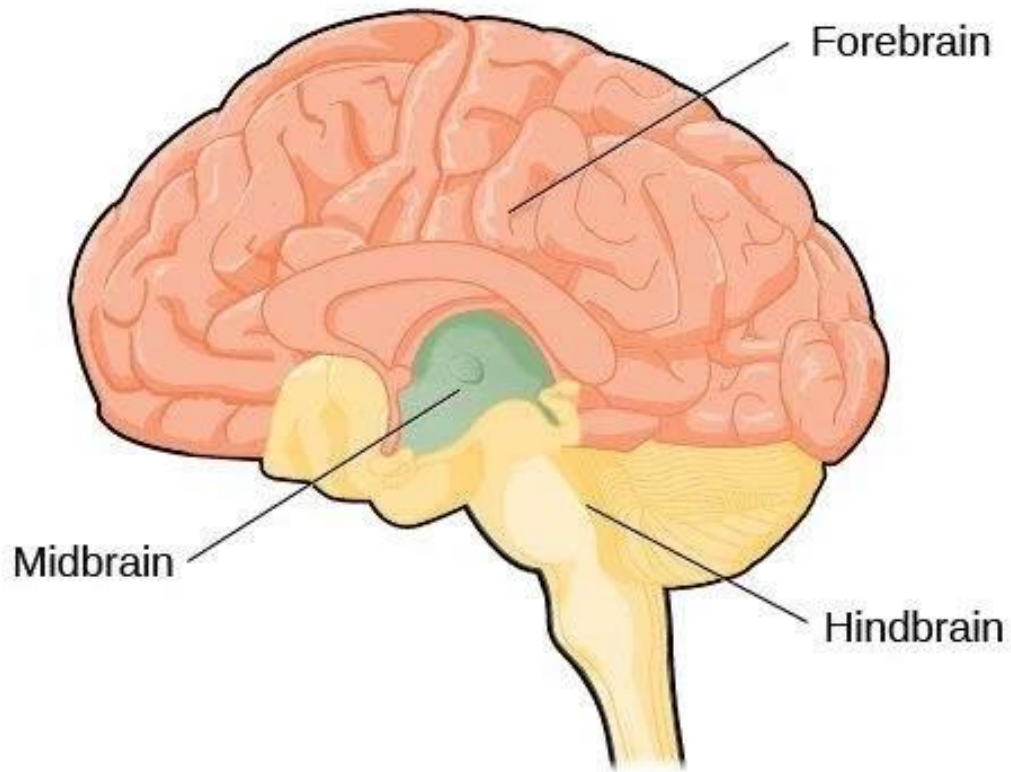
Figure 1. Parts of the human brain (Source: Eid, 2023).

2.1.1 Left Temporal Region

The temporal lobe of the brain is on both sides of the brain. The left temporal region is on the left side of the head. The left temporal region plays a major role in processing auditory information. It is also crucial for memory and emotional tasks. Generally, in right-handed people, the left temporal region is responsible for speech and comprehension tasks. If the left temporal region is damaged, there is a high probability of impairment in abilities such as speaking, understanding, reading, and writing.

2.1.2 Right Temporal Region

The part of the temporal lobe on the right side of the brain is called the right temporal region. It also plays an important role in processing auditory information, memory formation, and emotional information as well as facial recognition.

2.1.3 Anterior Region

It is located in the front of the brain and is a part of the frontal lobe. The integration of internal and autonomic data with emotional, cognitive, and motivational processes is facilitated by the anterior region.

2.1.4 Cental Region

It is used to describe the middle, anterior, and posterior regions of the brain. The brain, which is a very complex structure, does not have a single center.

2.1.5 Posterior Region

It is a term used for the back side of the brain. It has many important structures. Processing visual information received from the eye by interpreting the visual stimuli is its most important task.
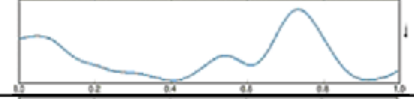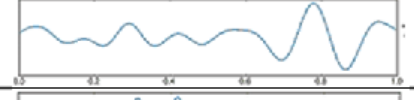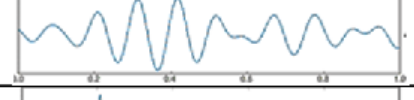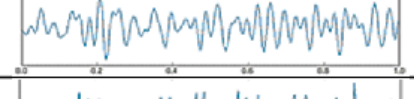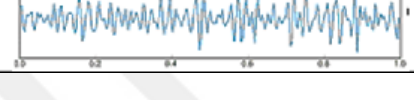
2.2 EEG

The Electroencephalogram (EEG) is a method for recording the electrical activity of the human brain using electrodes placed on the human scalp. The German psychiatrist Hans Berger was the first to record the electrical field of the human brain and he invented the EEG. The EEG has been helping with the diagnosis of many neurological diseases for many years. The low cost of the EEG was one of the main reasons that made it a popular and widespread technique (Shamsi et al., 2022). In a healthy brain, EEG coherence decreases as the distance between recording electrodes increases (Comi et al. 1998). This is important for the early diagnosis of neurological diseases amongst them ADHD. Many methods are used to evaluate EEG signals. In academic studies, EEG signals have been used for the classification of neurological diseases. Deep learning and machine learning methods were also used in this work of classification.

The EEG calculates the potential difference of electricity in the brain. Small electrodes are placed on either side of the scalp, by sticking them through a conductive material

called "paste". It transmits different frequency subbands such as delta (δ), theta (θ), alpha (α), beta (β), and gamma (γ), as shown in table1.

Table1. The frequency bands of EEG signals (Source: Oon, Saidatul and Ibrahim, 2018)

Waves	Frequency bands (Hz)	Behaviour Trait	Signal Waveform
Delta	0.3 − 4	Deep sleep	
Theta	4 − 8	Deep Meditation	
Alpha	8 − 13	Eyes closed, awake	
Beta	13 − 30	Eyes opened, thinking	
Gamma	30 and above	Unifying consciousness	

2.3 Literature Review

Classically ADHD diagnosis with the help of the EEG is done by neurologists but their method is very time-consuming because they study the EEG signal for a long period. Unfortunately, that method has been proven to give incorrect results with a high probability. The literature discusses various signal-processing methods to solve this problem concerning the diagnosis of ADHD or other neurological diseases such as epilepsy, dementia, etc. Various signal-processing techniques have also been used in the literature for ADHD classification. One of the most popular of these is the Fourier Transform (FT). FT is ideal when the signal is stationary. If the signal is non-stationary, FT assumes the signal is stationary. But neither signals from the real world nor EEG signals are stationary. This approach constitutes a huge disadvantage of the FT. In addition, FT does not contain time-relevant information. This is why other methods were developed, for example, the Short-Time Fourier Transform (STFT) which uses only one filter. Another method uses various filters with different bandwidths named the Wavelet Transform (WT). The approach of WT offers multiresolution. WT uses a

window containing all signals. In the first step, it subtracts low frequencies. The result is then converted and scaled again to extract high-frequency information. Despite all these advantages, the main disadvantage of WT is its lack of simultaneously improved time and frequency resolutions. To overcome this problem, the Empirical Mode Decomposition (EMD) algorithm was developed. EMD is an alternative method to analyze non-linear and non-stationary signals by producing a limited number of amplitude and frequency-modulated oscillations called intrinsic mode functions (IMFs) (Amado-Caballero et al., 2023). When you add up all the IMFs that were generated, the signal itself can be reproduced. Compared to WT, which analyzes the signal as a whole and is based on predetermined filter scales, EMD has the advantages of adaptable scales, data-driven oscillation separation, and local multi-resolution analysis.

The Intrinsic time-scale decomposition (ITD) algorithm is used for ADHD classification. ITD is used for the analysis of non-linear signals. Using the ITD algorithm, ITD modes called Proper Rotation Components (PRCs) are created. Machine learning techniques were developed, that use different combinations of PRCs for the classification of ADHD. These machine learning methods are the so-called Decision trees (DT), the Naive Bayes (NB), the Support vector machine (SVM), and the k-nearest Neighbor (KNN). In this study, 88.06% and 99.06% accuracy was achieved (Cura, Atli and Akan, 2023). Another study classified ADHD patients using the Douglas–Peucker Algorithm (Akan et al., 2022). In that study, 91.01% accuracy was obtained. In another ADHD classification, classification was made with the help of convolutional neural network (CNN) using EEG feature maps and classification was also made with certain machine learning algorithms. Additionally, the Long Short-Term Memory (LSTM) algorithm was used obtaining an accuracy between 84.99% and 99.75% (Akan et al., 2023). In most academic studies, the One-dimensional convolutional neural network (1D CNN) is used to classify raw EEG data but as long as no additional signal processing technique supported the findings, the accuracy was low. In some studies, densely layered 1D CNN was used. Even using raw data in this study, good results were obtained, averaging, an accuracy rate of 95.83% (Jahed et al., 2022). In another study, the Dynamic frequency warping (DFW) algorithm was used to classify ADHD. By extracting certain features and classifying them using KNN and SVM machine learning techniques 99.17% accuracy was obtained (Shamsi et al.,

2022). In another study, the resting state of a patient was classified with the help of 4D-CNN using functional magnetic resonance imaging (rs-fMRI) obtaining 71.3% accuracy (Yue et al., 2019). With certain exceptions in academic studies, using 1D-CNN in ADHD classification achieved no high accuracy. Better results were often obtained as a result of applying certain signal processing techniques to the EEG signal. Therefore, using raw EEG data will result in a lower accuracy.

In this study, certain noises were removed by Butterworth filtering the EEG signals taken from ADHD patients. Then the signal was decomposed into 5-second windows and the first five IMFs of the signal were obtained with the help of the EMD algorithm. Spectrograms of these 5-second signals were taken. This process was applied to the EEG signals of all patients and control group in the data set. Then, all these images were classified with two different 2D-CNN architectures developed in the Python environment. In addition, the ready-made architecture of Matlab was also classified with ResNet-50. In addition, while creating the data set in this study, EEG signals were taken from the anterior region, left temporal region, right temporal region, central region, and posterior region of the brain. The data received from these regions are classified among themselves. In this way, it was determined which part of the brain was more suitable for ADHD classification.

2.4 ADHD

ADHD as a neurological disease causes psychiatric disorders at a rate of approximately 70% (Tor et al., 2021). These psychiatric disorders include behavioral difficulties, depression, and anxiety. Due to all these difficulties, patients' quality of life decreases. ADHD patients are unsuccessful in their adult academic and business lives. The disease usually lasts throughout the whole life. Their families carry a long-term burden. Therefore, early diagnosis of the disease is very important. Between 5% and 7% of the children worldwide suffer from ADHD. Among adults, the percentage decreases to approximately 2.5% (Amado-Caballero et al., 2023). It is estimated that between 3.3% and 4.4% of US adults have ADHD (Kenter, Lundervold and Nordgreen, 2021). This rate is the ratio of reported patients to the entire population. Research shows that ADHD is more common in childhood boys than in childhood girls. The prevalence rate of this disease among men and women in adulthood is

approximately 50%. Once the disease is diagnosed, usually drug treatment ensues. However, since some patients are intolerant to medications and also suffer from side effects such as decreased sleep and appetite, psychological methods are also part of the treatment from time to time. It can be said, that ADHD is conducive to both pharmacological and psychological treatment methods (Yaghoobi Karimu and Azadi, 2018). However, the pharmacological method is preferred.

Since the method of machine learning has become popular for classification in recent years and graphics processing units (GPUs) have become stronger and cheaper, the classification of neurological diseases can be more easily made. Using deep learning, a sub-branch of machine learning, for these classification processes has increased. Especially nowadays, as GPUs become more powerful and easy to access, the classification of neurological diseases with the help of a deep learning technique is no longer a time-consuming process. For all these reasons, it should be obligatory to use deep learning techniques in the classification of neurological diseases. In this thesis study, classification is performed with 2D-CNN, which is a deep learning architecture.

CHAPTER 3: MATERIAL and METHOD

In this section, the EMD algorithm used for signal analysis and the 2D CNN architecture used for classification are introduced.

3.1 Empirical Mode Decomposition

In this thesis, Empirical Mode Decomposition (EMD), an advanced signal processing method, is used. EMD is used for biomedical data analysis. It was introduced in 1998 by Huang et al (Huang et al., 1998). Thanks to EMD, EEG segments are distinguished. Intrinsic Mode Functions (IMF) are obtained using EMD. IMFs are used in linear and non-stationary cases. It has a noise reduction feature. It brings out features in its applications. The sum of all IMFs gives the original signal (Mert and Akan, 2014). To ensure the IMF position, first of all, the number of extrema and zero crossings should either vary by one or be equal. The second condition is that the average value of the upper and lower envelopes must be zero. The IMF extraction process is shown in Algorithm 1. As in Figure 2, signals from IMF 1 to IMF 5 are visible, and the EEG signal is also visible. Figure 2 is taken from the patient group. Figure 3 is taken from the control group and the signals from IMF1 to IMF 5 are visible as in figure 2, and the EEG signal is also visible. Figure 4 is the FFT version of the signals in Figure 2. Figure 5 is the FFT version of the signals in Figure 3.
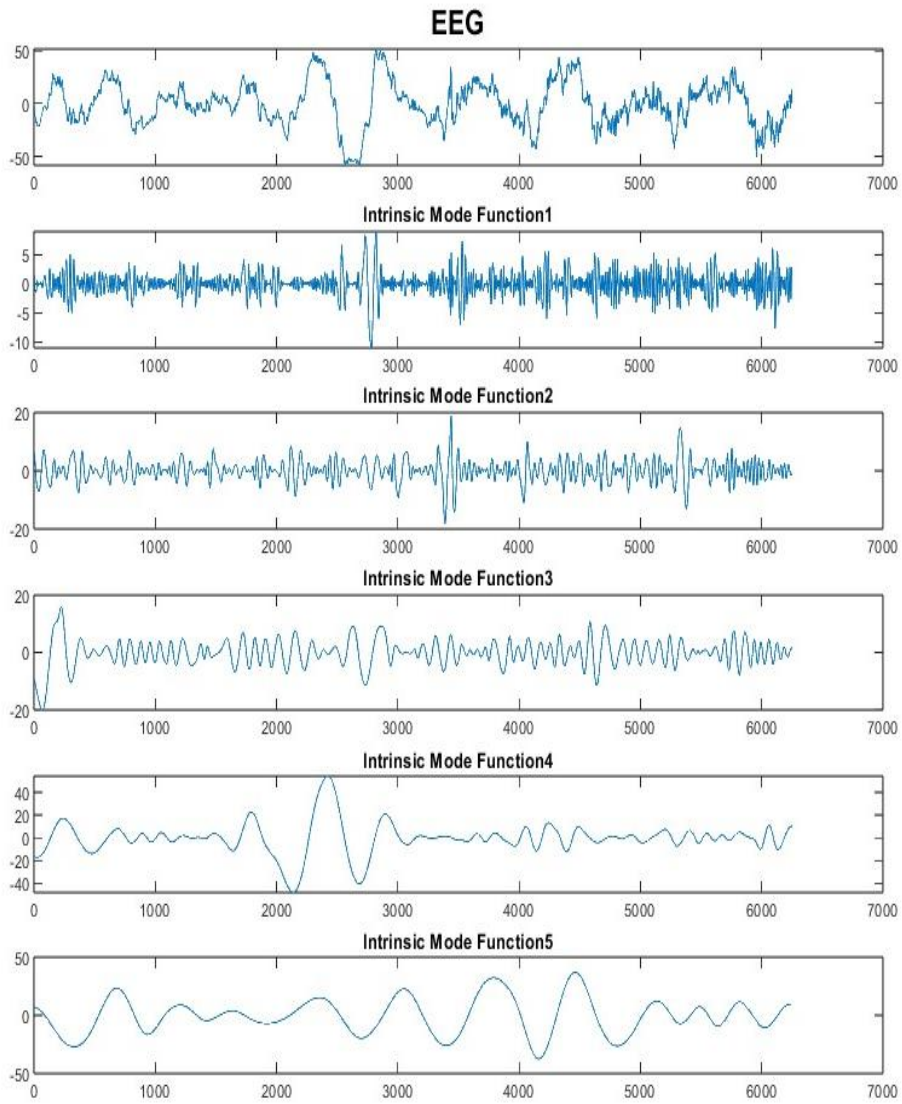
Figure 2. 5-second EEG signal and IMFs taken from the patient
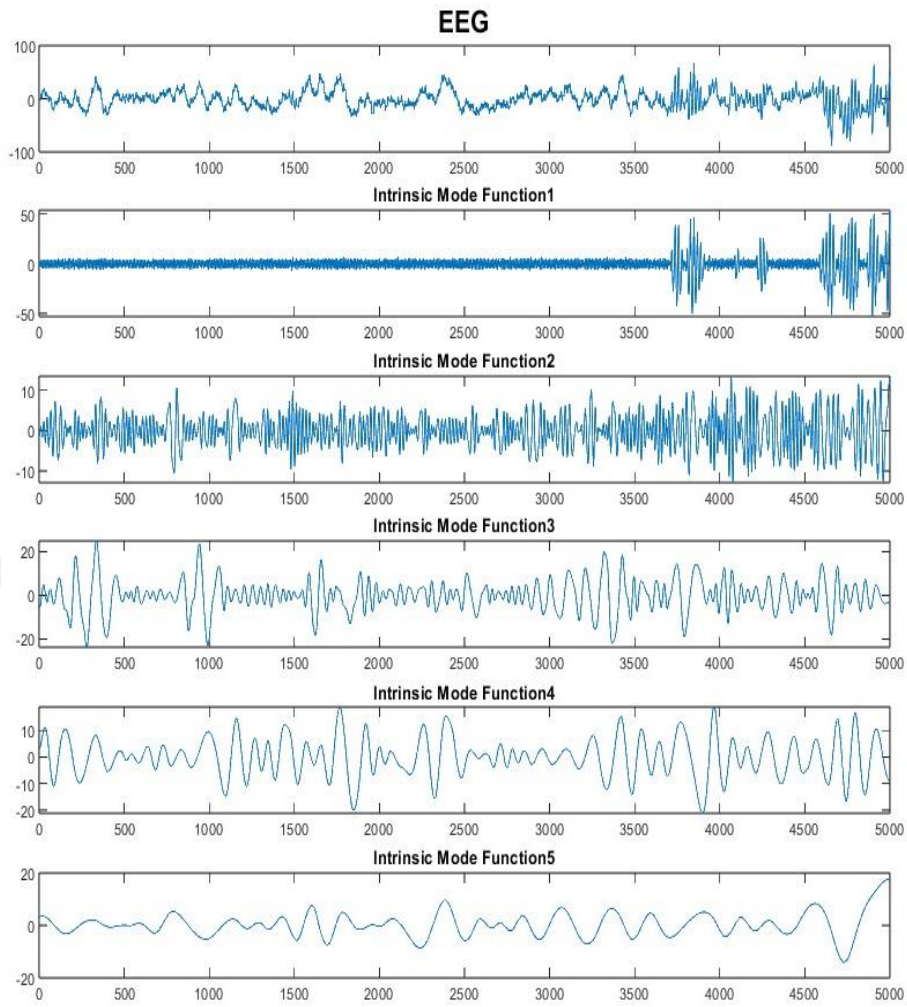
Figure 3. 5-second EEG signal and IMFs taken from the control

Algorithm 1: EMD

1. Local minima Lm_i, $i = 1, 2, ...$ and Local maxima Lx_j, $j = 1, 2, ...$ are found using input signal $x[n]$.

2. Calculate $Ue[n]$ and $Le[n]$ which upper and lower envelopes respectively, using cubic interpolation.
3. Mean of envelopes value is found.

4. Compute $d_1[n] = x[n] - Me[n]$. If $d_1[n]$ satisfies the condition of IMF,

$d_1[n] = IMF_1[n]$. Else go to step 1 and repeat every processes using $d_1[n]$ instead of $x[n]$.
5. After obtaining $IMF_1[n]$ calculate the residue $R_1[n] = x[n] - IMF_1[n]$. If this residue has more than a zero-cross, return step 1 and calculate again new IMF.

This process will continue until last residue $R_L[n]$ which has no zero cross is obtained and all necessary conditions are satisfied.

We can reconstruct the original signal $x[n]$ using the following formulation:

$$x[n] = \left(\sum_{l=1}^{L} IMF_l[n] \right) + R_L[n]$$

Here, L is the number of $IMFs$ and $R_L[n]$ is the residue.
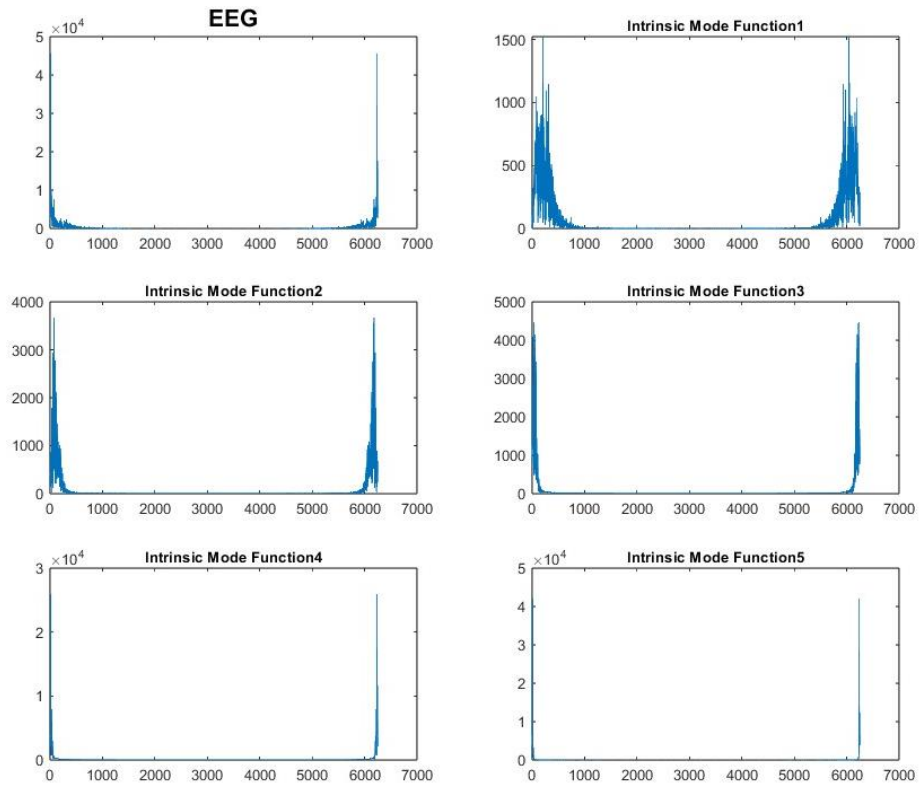
Figure 4. 5-second EEG and IMFs FTFT taken from the patient
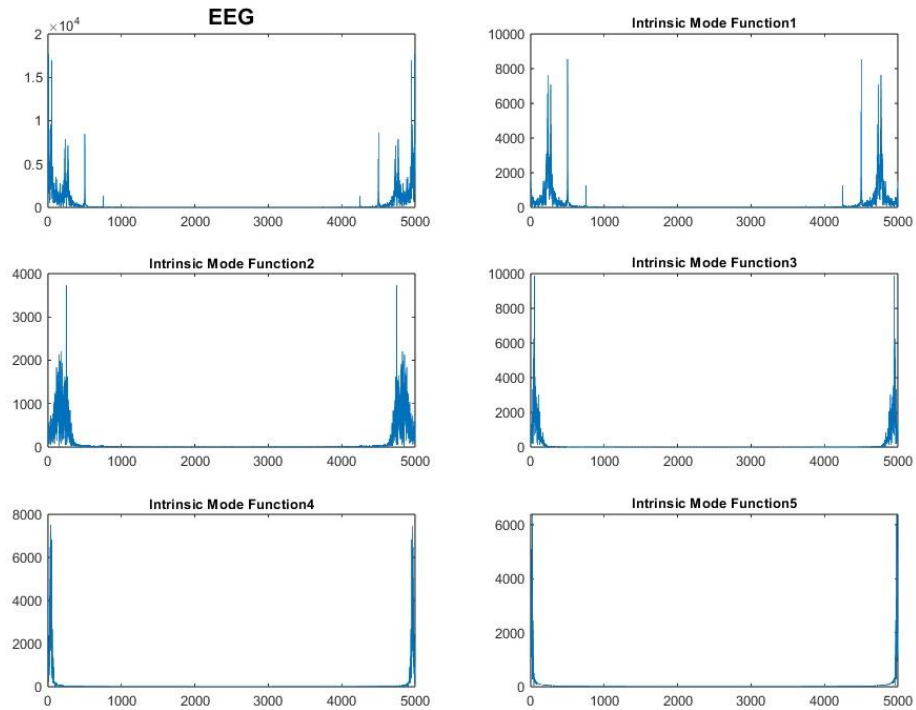
Figure 5. 5-second EEG and IMFs FFT taken from the control

3.2 Spectrogram

Short-time Fourier transform (STFT) is the most widely used method for examining non-stationary signals (Cura and Akan, 2021). When performing STFT, it divides the signal into small time segments and Fourier determines the frequencies present in that segment. The integrity of such spectra shows how the spectrum changes over time. A spectrogram is a two-dimensional plot in which the horizontal axis represents the frequency range of the spectral content and the vertical axis represents time. It is a visual representation of the frequency spectrum of the signal. The signal displayed must be a time-varying signal. The spectrogram plot is always represented as a 3D plot. Spectrograms are used in many areas. Some examples are linguistics, seismology, speech processing, sonar, and radar. A spectrogram is displayed as a heat map. In the Figures 6 to 17 shown, red represents the densest parts and blue represents the least dense parts. It is two-dimensional as in Figures 6 to 17. One axis represents time and the other represents frequency. The third dimension, the dimension indicating amplitude, is represented by colors. There is more than one plotted version of the

spectrogram. Creating a spectrogram using STFT is a digital process. Continuous-time STFT is as given in equation 1. Discrete time is as given in STFT equation 2. The spectrogram is as given in equation 3. Figure 17 shows the spectrogram of the EEG signal taken from the control data set. IMFs of the same signal are seen in the images from Figures 6 to 10. As in Figure 6, the red lines are above because the IMF1 contains the highest frequencies of the EEG signal. In the later IMF2, the red levels go down a little more. Each figure exhibits a gradual decrease in its distinguished frequencies. Finally, IMF5 contains the lowest frequencies. Figure 16 shows the spectrogram of the EGG signal taken from the patient data set. The pictures from Figure 11 to Figure 15 are IMFs of the same signal.

$$\mathbf{STFT}\{x(t)\}(\tau, \omega) \equiv X(\tau, \omega) = \int_{-\infty}^{\infty} x(t)w(t-\tau)e^{-i\omega t}\, dt \tag{1}$$

$$\mathbf{STFT}\{x[n]\}(m, \omega) \equiv X(m, \omega) = \sum_{n=-\infty}^{\infty} x[n]w[n-m]e^{-i\omega n} \tag{2}$$

$$\mathrm{spectrogram}(t, \omega) = |\mathrm{STFT}(t, \omega)|^2 \tag{3}$$
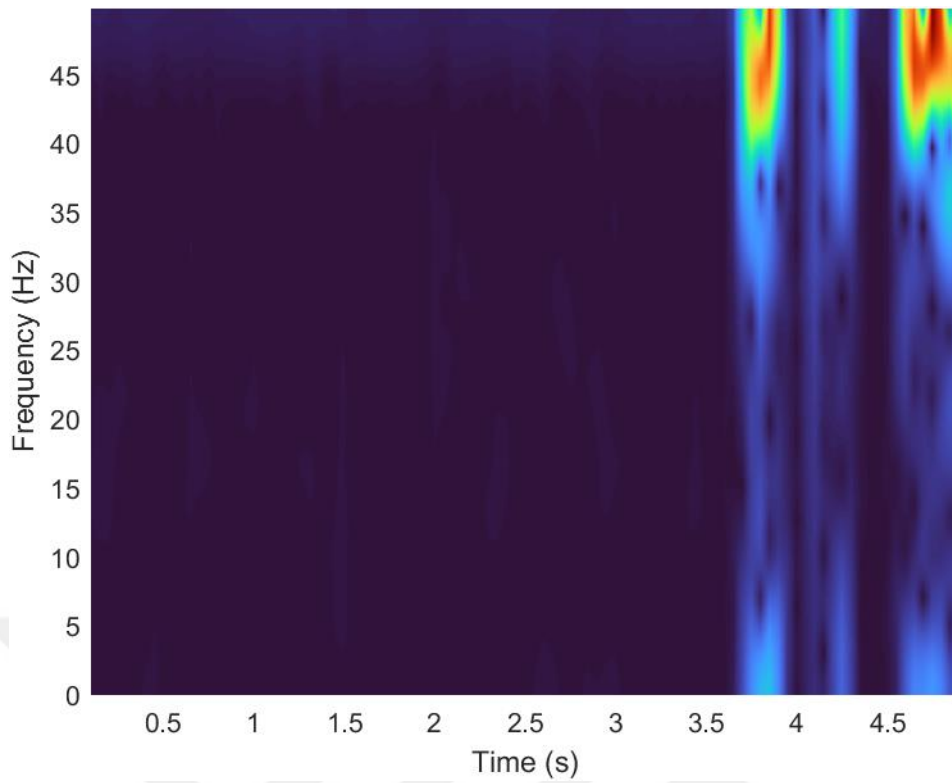
Figure 6. IMF1 spectrogram example from the control data set

Figure 7. IMF2 spectrogram example from the control data set
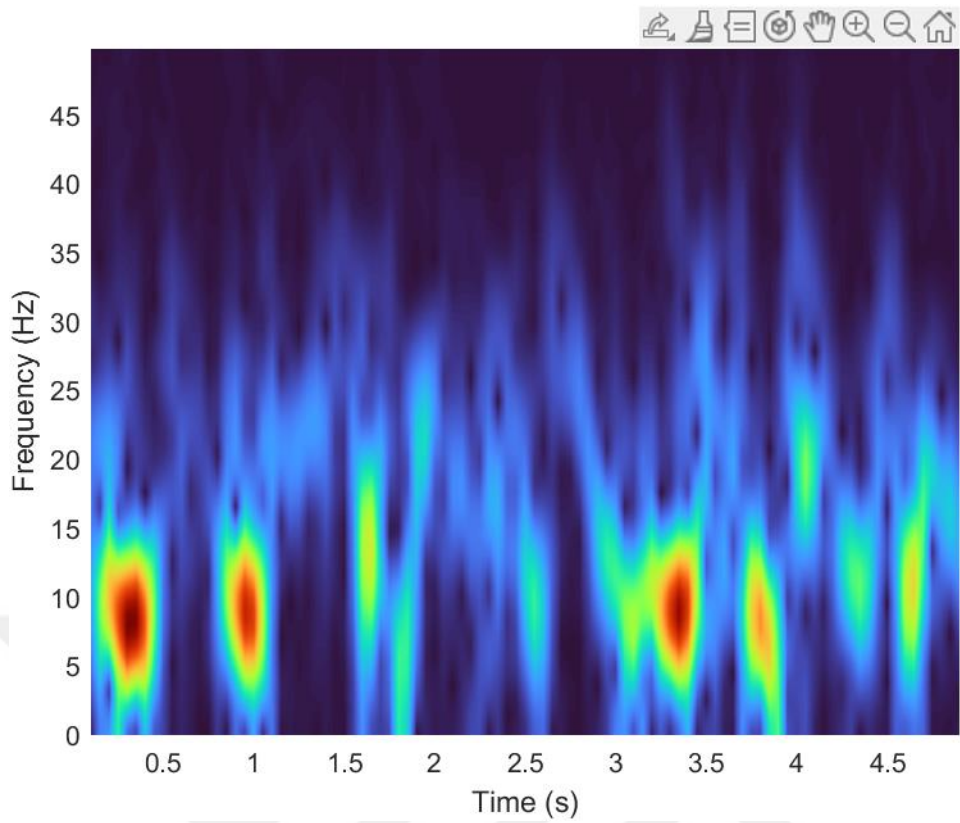
Figure 8. IMF3 spectrogram example from the control data set
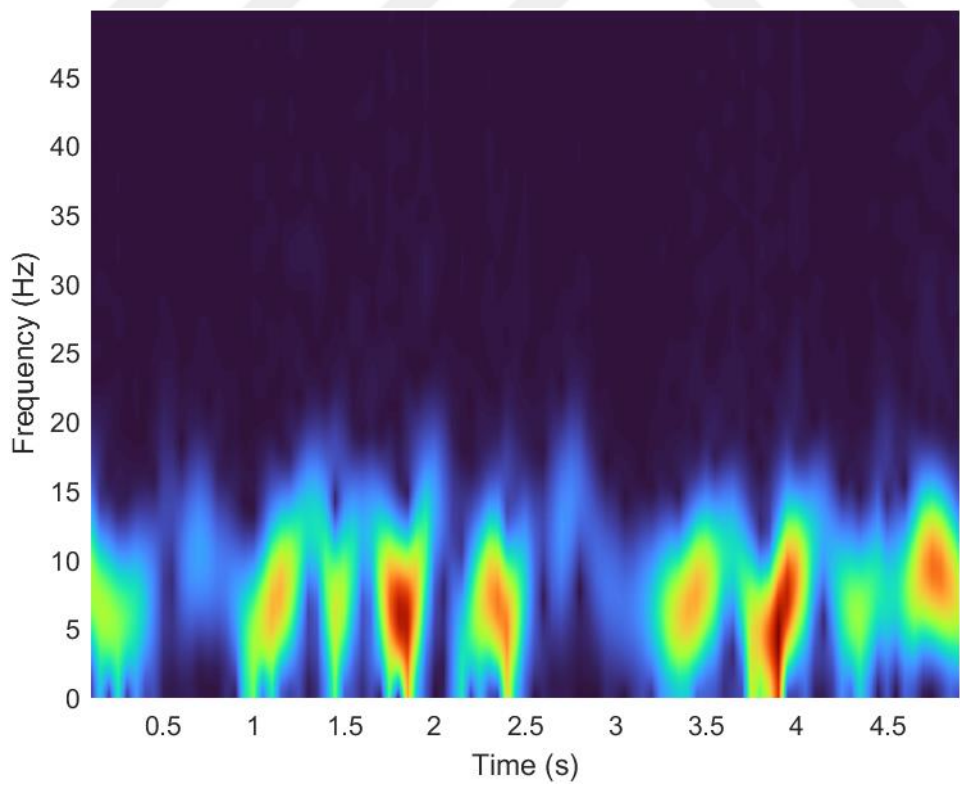
Figure 9. IMF4 spectrogram example from the control data set
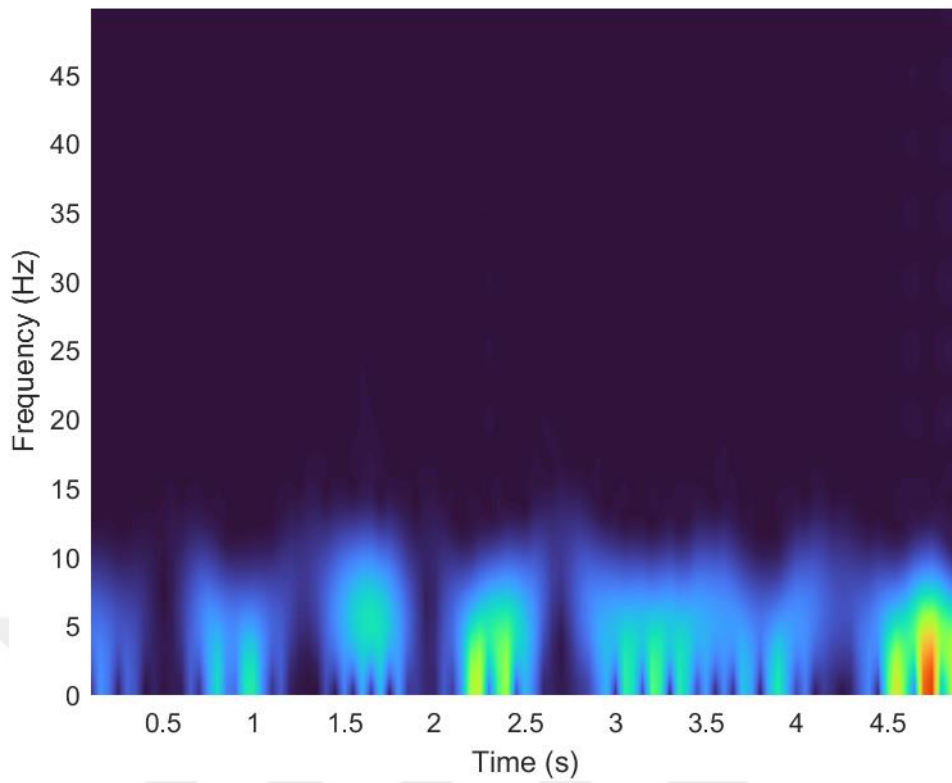
Figure 10. IMF5 spectrogram example from the control data set
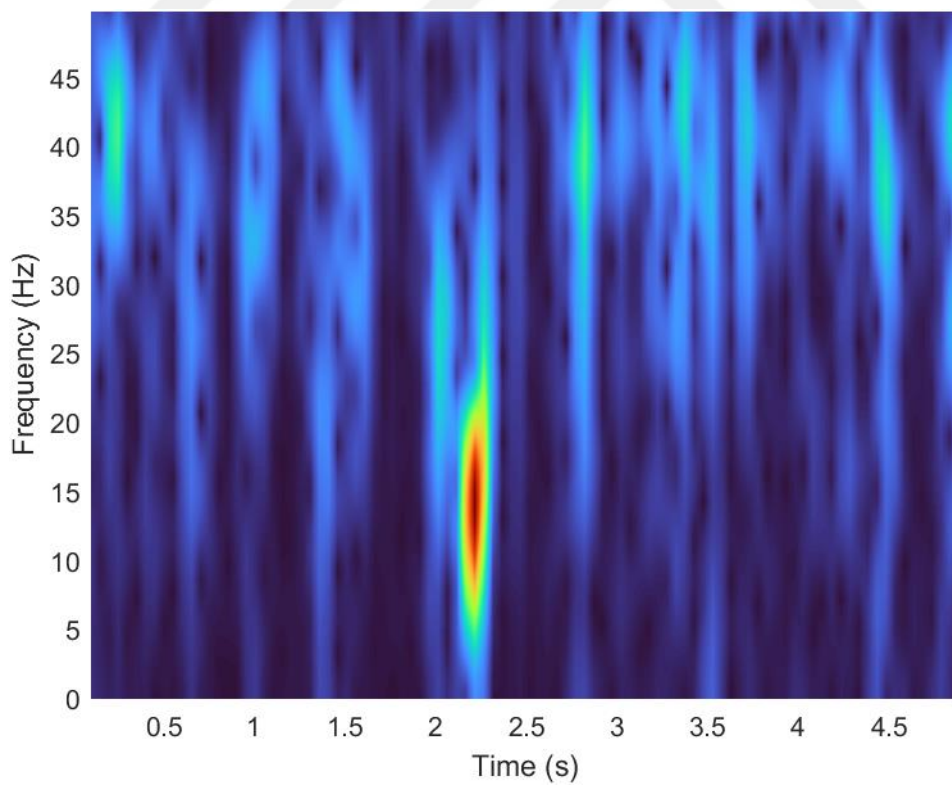
Figure 11. IMF1 spectrogram example from the patient data set
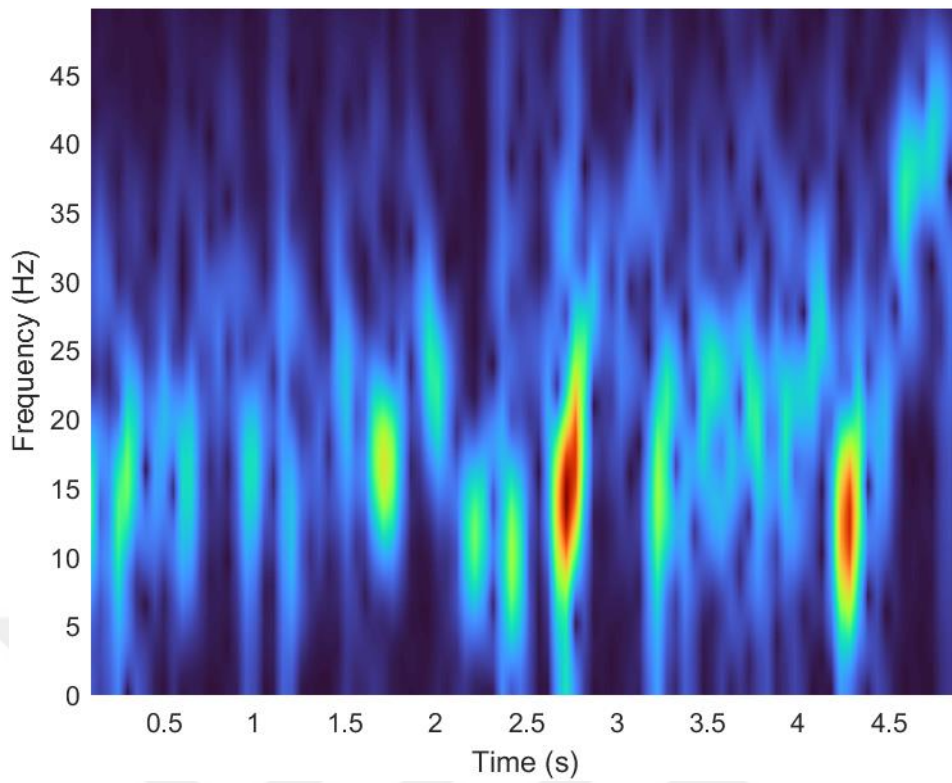
Figure 12. IMF2 spectrogram example from the patient data set
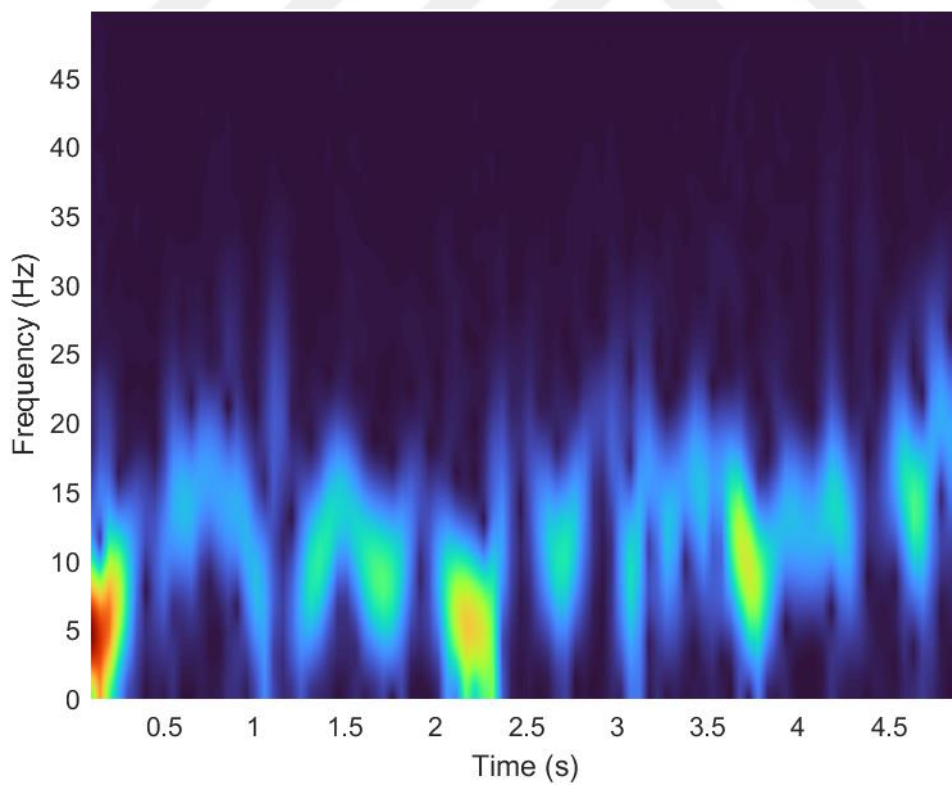
Figure 13. IMF3 spectrogram example from the patient data set
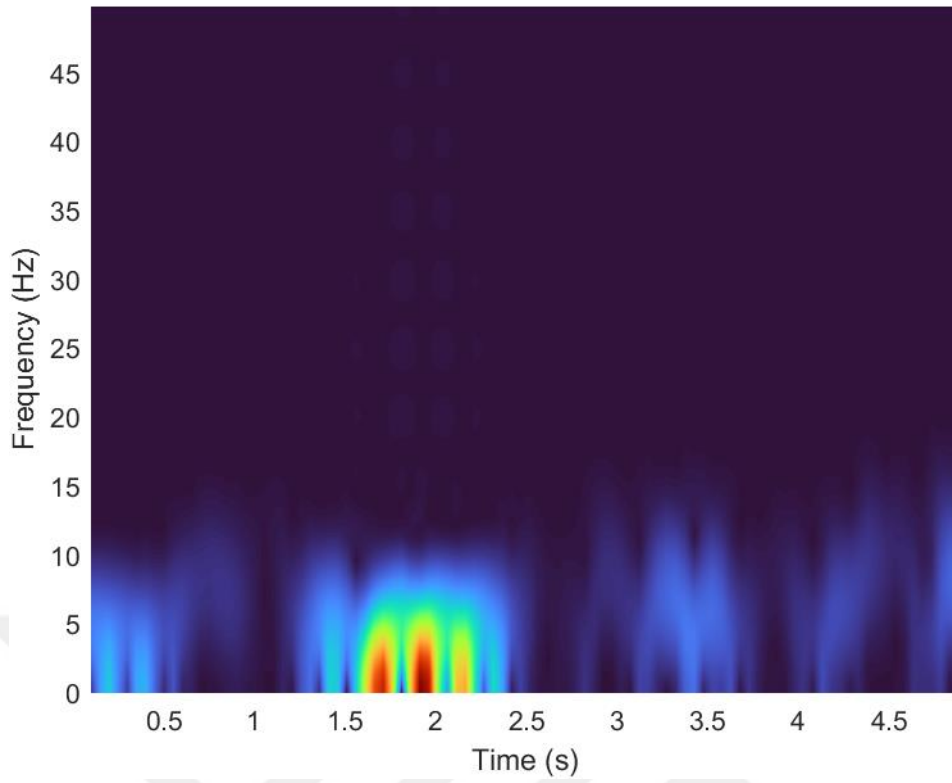
Figure 14. IMF4 spectrogram example from the patient data set

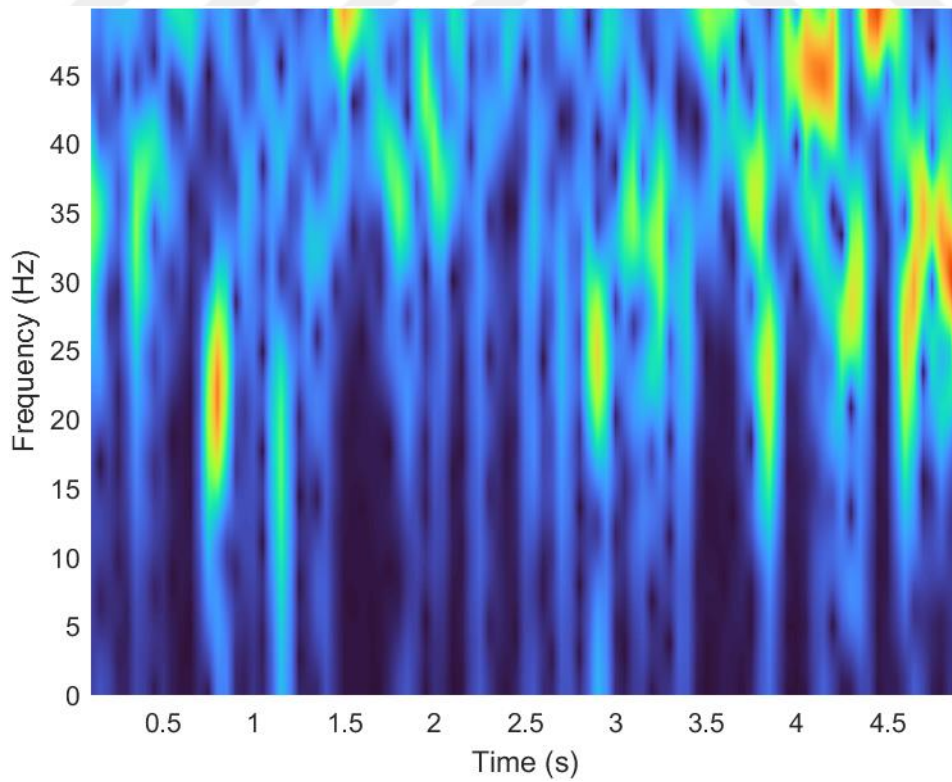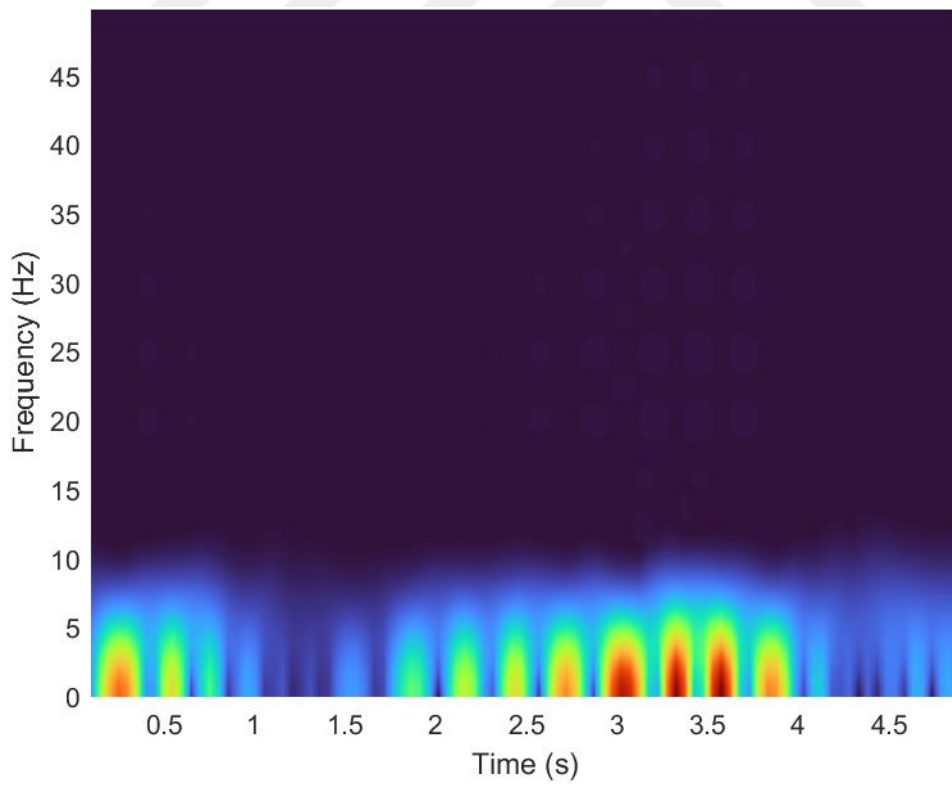Figure 15. IMF5 spectrogram example from the patient data set
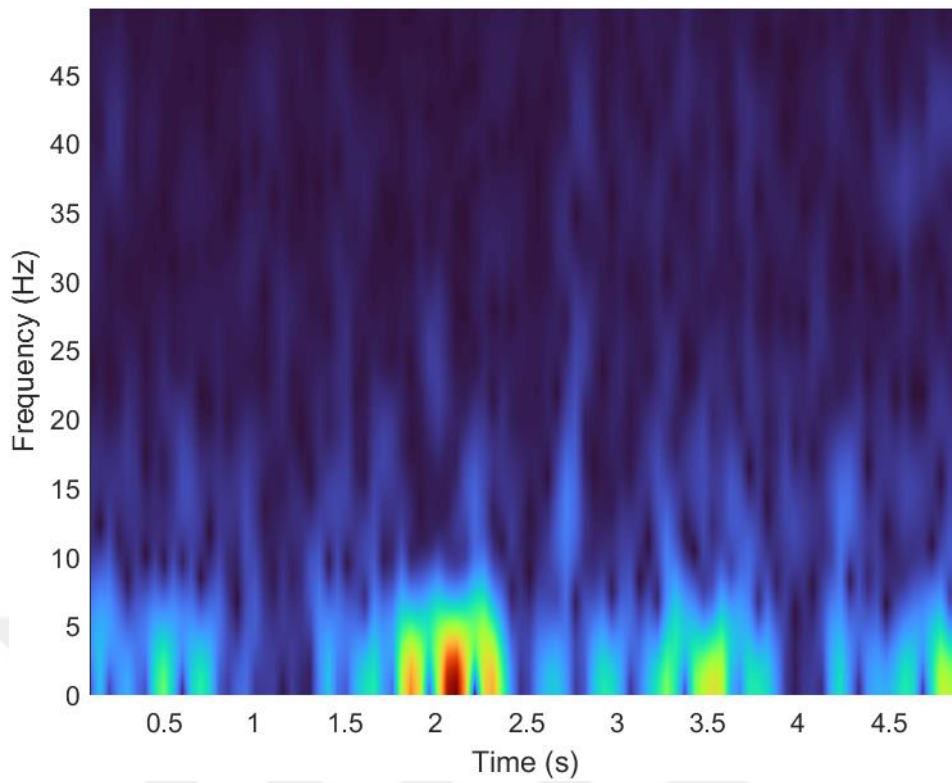
Figure 16. EEG spectrogram example from the patient data set
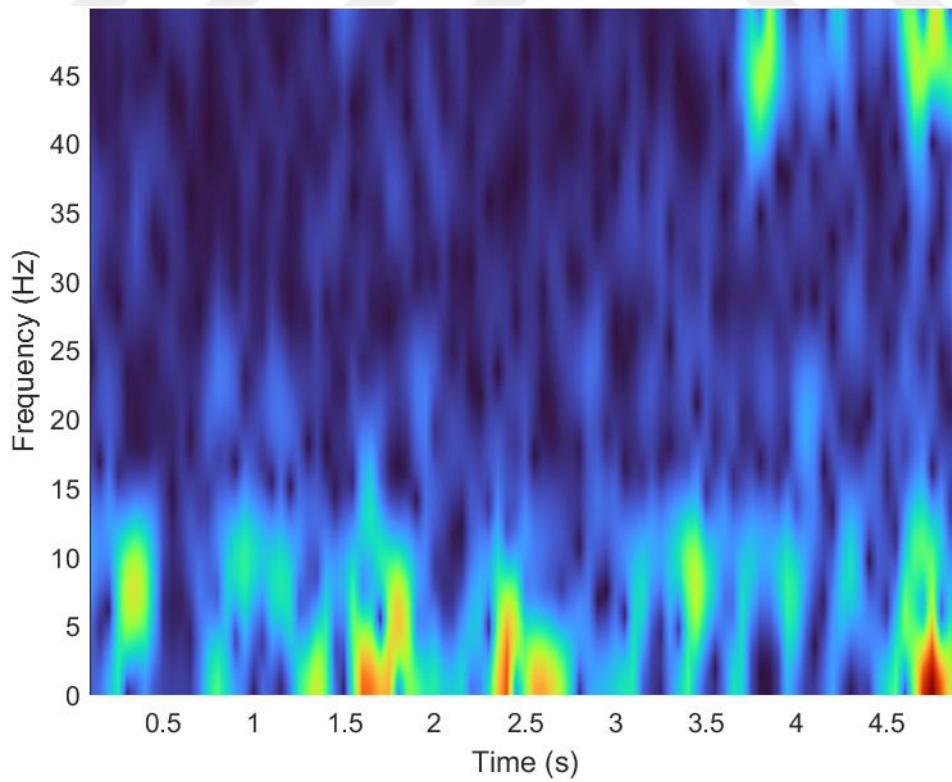
Figure 17. EEG spectrogram example from the control data set

3.3 Deep learning

Deep learning, which started with Artificial Neural Network (ANN), is a very old concept. Deep learning was not a popular field before. But today, it has become a popular field thanks to the fact that Graphics processing units (GPU) are becoming more powerful and cheap. These developments have made deep learning a very important field of research. Its working system is similar to the human nervous system. Deep learning is a sub-branch of machine learning. Deep learning, also known as deep neural networks, has many layers. Neural networks can learn and represent hierarchical features. Today, deep learning is used in many areas such as image and speech recognition, natural language processing, medical diagnosis, and autonomous vehicles. Convolutional Neural Network (CNN), which is the most used deep learning architecture today, performs classification. Additionally, CNNs are widely used in biomedical and medical fields today. CNNs are specialized neural networks designed to process grid-like data such as images. A typical CNN architecture includes input and output layers, as well as three main hidden layer structures: convolutional, pooling, and fully connected layers. CNN is a deep learning algorithm based on artificial neural network structures. The input layer is the size of the data. The output layer is equal to the number of classes. If the number of classes is 2, the number of output layers can be 1. The structure is inspired by the brain's working system, which contains many hidden layers. Neurons enable feature detection from input data.

CNNs are used in many areas such as image and video recognition, recommendation systems, image classification, image segmentation, medical image analysis, natural language processing, and brain-computer interfaces. A Convolutional Neural Network is also known as ConvNet. Digital images consist of pixels. Each pixel has a mathematical equivalent. CNNs can also classify audio and signal data.

3.3.1 Convolution Layer

In convolution there is a small set of numbers called a kernel. Usually, it is 3 x 3. It is also used in 5 x 5 and 7 x 7 studies. A sequence of numbers called a tensor is applied across the input. The values of the tensor and the kernel are multiplied and the resulting values are added. The result becomes our output value. Convolutional layers convolve the input and pass its result to the next layer. Convolution is a linear operation.

3.3.2 Nonlinear Activation Function

A non-linear activation function is the next operation after convolution. The most popular nonlinear activation function today is the rectified linear unit (ReLU). There are also non-linear activation functions such as sigmoid or hyperbolic tangent (tanh) function. ReLU has high adaptability to the training set. It has a huge impact on the performance of large models trained on large datasets.

3.3.3 Max Pooling

Max pooling is a commonly used subsampling process in convolutional neural networks (CNN). It is applied after the convolution layer. Generally, 2 x 2 is an ideal window for Max pooling. It is used to reduce computational complexity and control overfitting.

3.3.4 Flatten

Flatten is used to convert multidimensional data into a one-dimensional array. It is used to convert 2D arrays into a single long continuous linear vector.

3.3.5 Dropout

It is an editing technique used in CNN. It is also used in other deep learning models. It exists to prevent memorization. Overfitting indicates that a model performs well on training data, however, it cannot be successful when tested with new data. Dropout is used to prevent overfitting.

3.3.6 Fully Connected Layer

It is often used at the end of network architecture to make predictions based on high-level features. When there are more than 2 classes, softmax is used for the activation function. When there are 2 classes, the sigmoid function is generally used.

3.4 Description of the EEG Dataset

In this study, 30-channel EEG data recorded with the Brain Vision EEG recording system at Izmir Katip Çelebi University using a sampling frequency of 1 kHz was used. The dataset was recorded from 2 different groups: control and patient. The control group is healthy people. The patient group is ADHD patients. The average age of the patient group is 12. It consists of 8 girls and 7 boys. There are 15 ADHD patients in total. The average age of the control group is 13. It consists of 14 girls and 4 boys in total. It consists of 18 people in total. 30 seconds of EEG data are recorded from each participant during an eyes-open resting state. There are 32 channels in total in the data set, but the last two channels are eye movement. That's why the first 30 channels were used. The sampling frequency of the Control dataset is 1000 Hz. The patient dataset is 2500 Hz.

The longitudinal and transverse channel pairs evaluated are as follows: There are 12 transverse channel pairs (FP1-FP2, F7-F8, F3-F4, FC3-FC4, FT7-FT8, T3-T4, C3-C4, CP3-CP4, TP7 - TP8, T5-T6, P3-P4 and O1-O2) and 20 longitudinal channel pairs (FP1-O1, F7-T5, F7-O1, FT7-TP7, FT7-O1, F3-O1, F3-P3, FC3- CP3, FC3-O1, FZ-OZ, FCZ-PZ, FP2-O2, F8-T6, F8-O2, FT8-TP8, FT8-O2, F4-O2, F4-P4, FC4-CP4 and FC4-O2). Transverse and longitudinal channel pairs are as in Figure 18. Izmir Katip Çelebi University Clinical Research Ethics Committee guaranteed ethical approval dated 11.07.2019 and numbered 76 for the collection of EEG data used in this study. The ethical approval form is given in Appendix B. The channels are placed on the hairy part of the scalp. The region of the brain where the channels receive data is shown in Figure 19
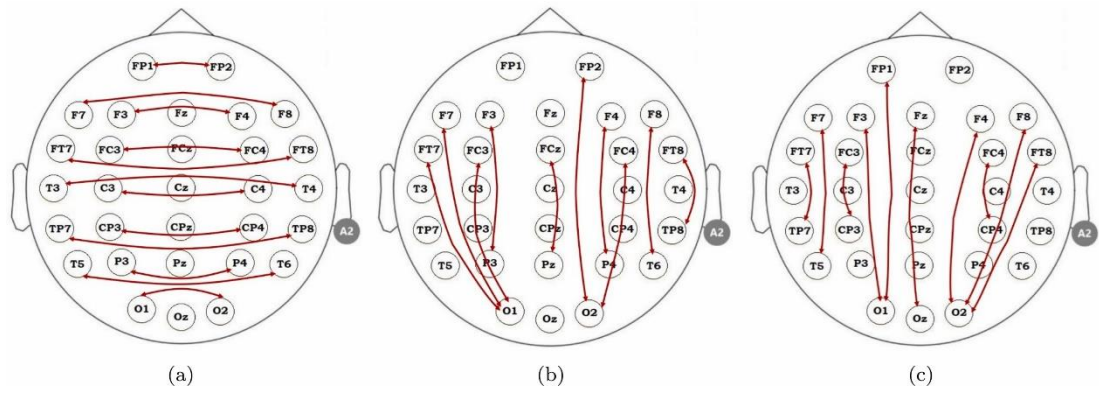
Figure 18. 30-channel brain electrode mapping (Source: Cura, Atli and Akan, 2023).
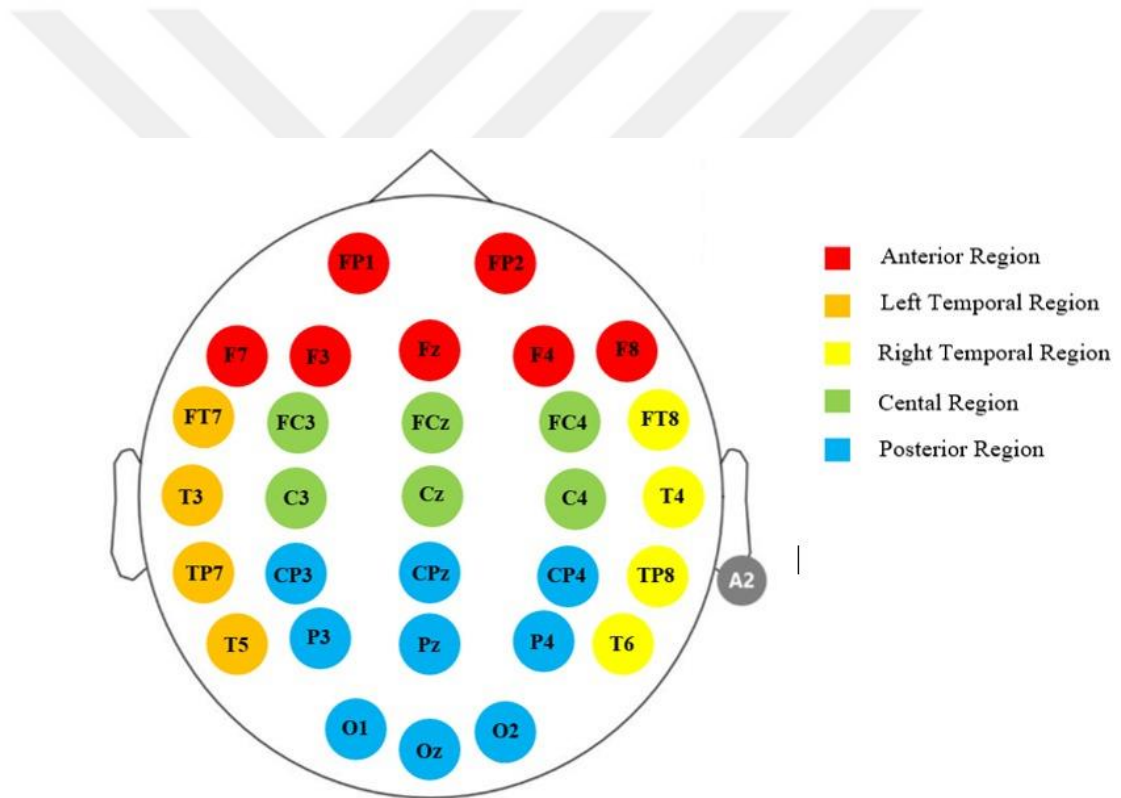
Figure 19. Channel positions at different brain regions.

3.5 Preprocessing of the EEG Dataset

First, the Butterworth filter, which is widely used in signal processing, was applied to all channels in the dataset to eliminate unwanted noise. Filter values were set at 0.6–

48 Hz. This filter was first used by the British engineer and physicist Stephen Butterworth in 1930.

Down-sampling is performed on the filtered dataset for the Patient Data. The reason for this is that the Patient data have a frequency of 2500 Hz and the Control data have a frequency of 1000 Hz. The Patient Data frequency was reduced to 1250 Hz. Downsampling is a digital signal processing technique. It preserves the signal's basic information but the data size is reduced. It is generally applied to audio and video processing. Productivity may increase at the end of the process. Since the frequency in the control data is 1000 Hz, they needed no downsampling.

After downsampling, the signal was decomposed into 5-second segments. There is no overlap in each 5-second window. Each 5-second sample was inserted into the EMD function. At the end of the process, the first 5 IMFs were acquired. Spectrograms of all IMFs and each signal passed through the filters were taken. The Hanning window was used while performing the spectrogram process. A total of 27420 images were created in the control dataset. In the Patient data set the same procedure was applied and it produced 21900 images. There are 49320 images in total for the entire dataset. Total data numbers for patients and controls are as in Figure 23, and the percentage distribution is as in Figure 22.
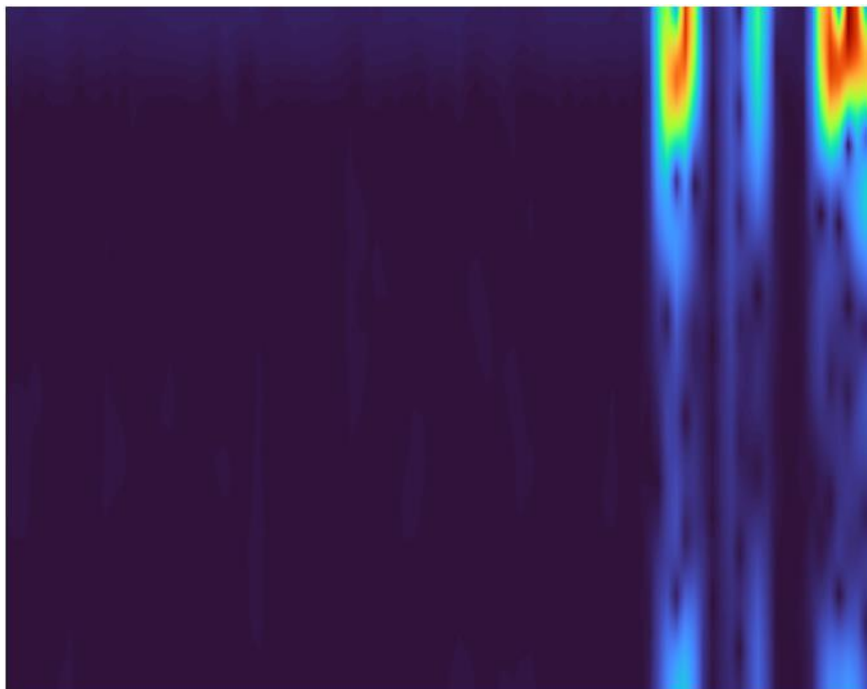
Figure 20. IMF1 spectrogram example from control data set for Deep Learning
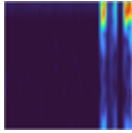
Figure 21. IMF1 spectrogram example from control data set for Deep Learning after Re-Size
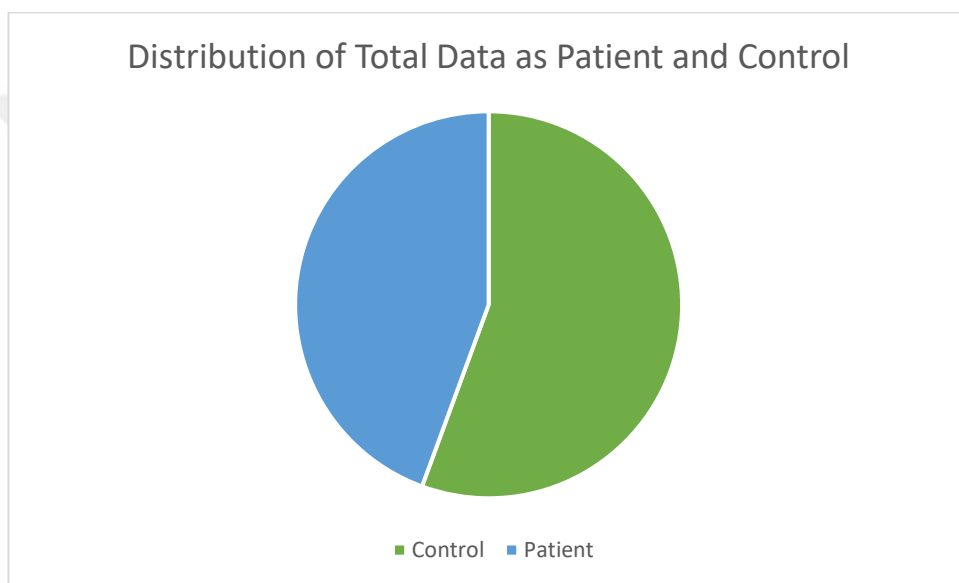
Figure 22. Distribution of total data as patient and control
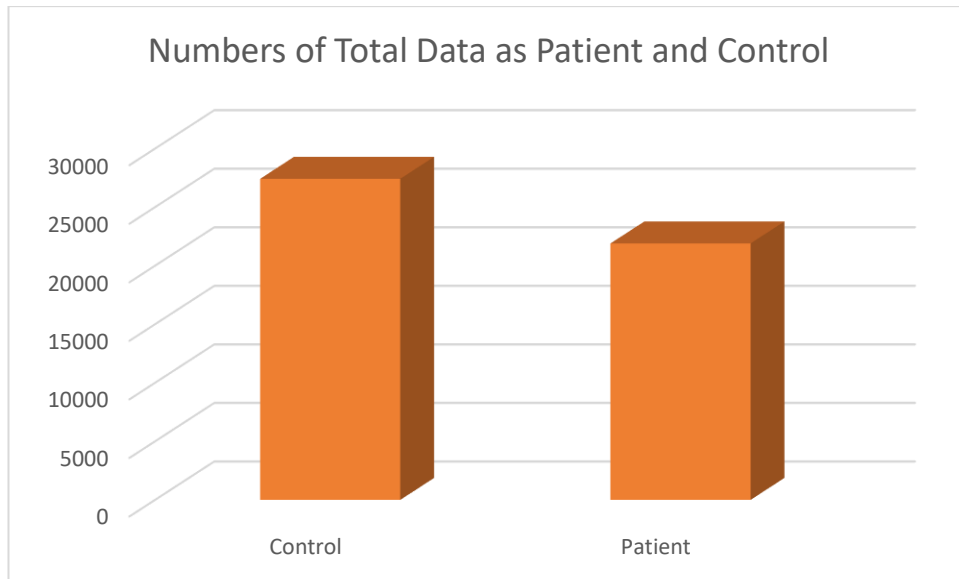
Figure 23. Numbers of total data as patient and control

 As in Figure 20, the size of each image is 683 x 539 x 3. The dimensions are 683 columns and 539 rows, and since the images are RGB, there are 3 channels. In total, there are about 1104411 pixels for each image. Considering the size of the total data set, this presents a large data set for CNN. Powerful hardware is needed to process this data set. Unfortunately, there is no powerful enough hardware available to process this dataset. Therefore, the images needed to be resized. Resize is the redimensioning of images or photographs. Images with a size of 683 x 539 x 3 have been reduced to 64 x 64 x 3 as in Figure 21. Unfortunately, in this case, a lot of data is lost, but in the absence of this process, classification with 2D-CNN is impossible with the available hardware. Images of size 64 x 64 x 3 were classified with 2D-CNN.

There are a total of 11508 images in the data set taken from the Anterior Region (AR). 6398 of these pictures belong to the control group and 5110 belong to the patient group. There are 6576 images resulting from the Left Temporal Region (LTR) and Right Temporal Region (RTR), 3656 of which belong to the control group and 2920 to the patient group. The Central Region (CR) yielded 9864 images. 5484 of these belong to the control group and 4380 to the patient group. There are 14796 images attributable to the Posterior Region. 8226 of these images belong to the Control Group and 6570 to the Patient group. The Patient Control distribution of the data set is the same in all trials. 44% of the total data set is Patient and 56% is Control as in Figure 22. The

Posterior Region covers the largest area in the data set, 30% of the total data consists of data taken from the Posterior Region. It is followed by the Anterior Region with 23%. 20% of the total data consists of data received from the Central Region. The Left Temporal Region and Right Temporal Region cover 13%. The percentage distribution of the regions in the data set is shown in Figure 25. The number of data by region is shown in Figure 24
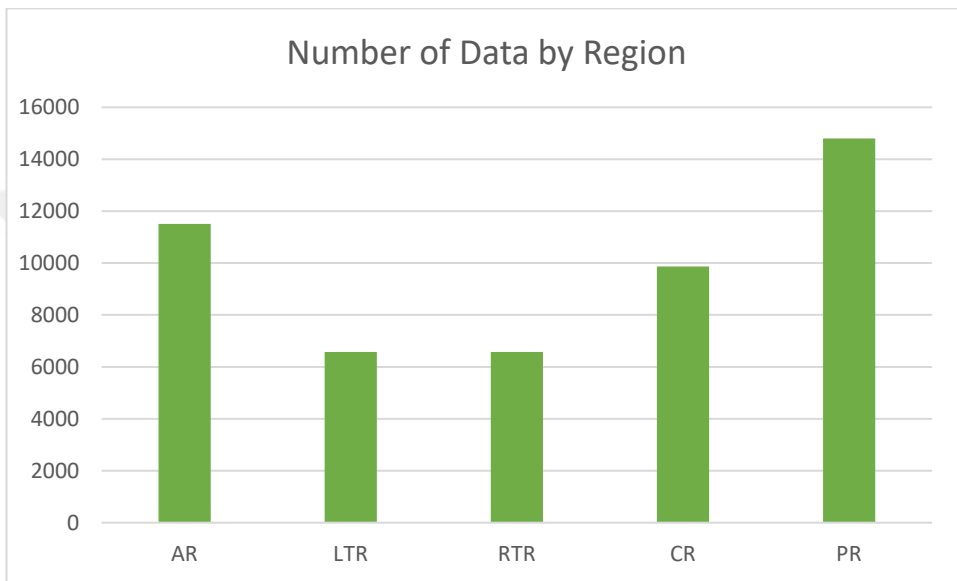
Figure 24. Number of data by region
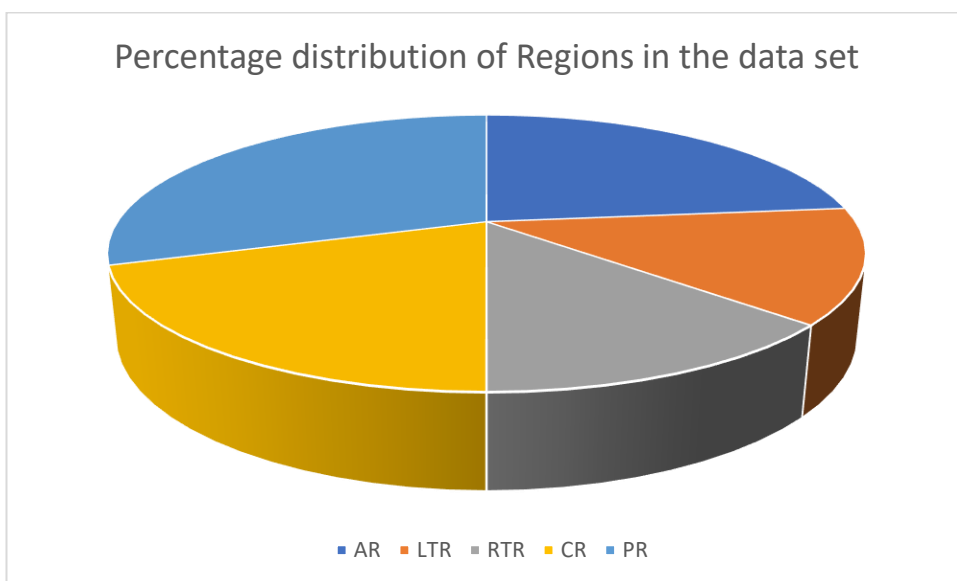
Figure 25. Percentage distribution of regions in the data set

3.6 Hardware of the Computers Used in the Study

In this study, 2 different computers were used. One of the computers used is a desktop. There is an AMD Ryzen5 5600x Central Process Unit (CPU), AMD Radeon™ RX 6700 XT Graphics Card, 16 gigabytes (GB) of 3600 (Megatransfers per second) Random Access Memory (RAM) in dual channel and finally a 2 terabyte Solid-state drive (SSD). Since the GPU does not support deep learning, only the processor is used in this computer. Therefore, it is more important to use a GPU with artificial intelligence (AI) support. The reason for this is that the data in this study is very large.

The second computer used is a laptop. The laptop Dell G5 15 5587 used in this experiment has the following hardware components: Intel Core i7-8750H CPU and Nvidia GTX 1060 Max-Q (6GB GDDR5) GPU are cooled with the stock cooler and Thermal Grizzly Conductonaut Liquid Metal is used as the thermal interface material to prevent any kind of thermal throttling. Also, the laptop has 16 GB of 2666 MT/s RAM in dual channel. The CPU is undervolved by 128 mV to prevent power throttling as much as possible. The clock speeds of 3.4 GHz for the CPU were maintained throughout this experiment. The graphics card in this computer has artificial intelligence support.

An area of approximately 182 GB is required for this work. The total size of all data covers approximately 182 GB. The largest amount of CNN's input data at a time is approximately 369 MB. These images are resized to 64 x 64 x 3 size. If the images are not resized, the space occupied by the input is approximately 7 GB. Since there was not enough hardware to process this data, the images were resized.

CHAPTER 4: EXPERIMENTAL RESULTS

In this part of the study, information about the experimental results is given. First, the EEG signals were passed through the Butterworth filter and then divided into 5-second non-overlapping windows. Later, the 1D data became 2D with the Spectrogram method. The signals were converted into images using the spectrogram method. In this case, correctly classifying the Patient and Control classes and which parts of the brain are more prone to ADHD classification are discussed in this part of the thesis. In this study, data from 5 different parts of the brain were classified separately with 3 different CNN architectures. Two of these architectures were designed in the Python environment. The last used CNN legacy is the Resnet-50 architecture, which is available in the Matlab environment. Today, many ready-made CNN architectures are used for the classification of neurological diseases. To give examples of these architectures, there are many ready-made architectures such as SqueezeNet, GoogLeNet, ResNet-50, EfficientNet-b0, Xception, Places365-GoogLeNet, Mobile-v2, DenseNet-201, VGG-16 and, AlexNet. In this study, experiments were made with all these CNN architectures. As a result of this study, only ResNet-50 achieved good accuracy. The others were not included in the study because their accuracy values were too low. In this thesis study, there are results about ResNet-50 and 2 different CNN architectures. Data taken from 5 different regions of the brain were classified among themselves, and classification was made using all the data. In this study, the spectrograms of the first 5 IMFs and the spectrograms of the original signal were classified separately. The dimensions of the images are 64 x 64 x 3 as mentioned in the previous sections.

4.1 Performance Evaluation Metrics

The success rate of the classification can be understood thanks to the Confusion matrix. The confusion matrix consists of true positive (TP), true negative (TN), false positive (FP), and false negative (FN) values. Since there are 2 classes in this thesis study, the Confusion matrix is a 2 x 2 matrix. If there were 3 classes, the matrix would be 3x3. This matrix ratio goes linearly. In this study, 2 x 2 confusion matrix results are available

in the experimental results section. The confusion matrix example is shown in Table 2.

Table 2. Confusion matrix

	Positive (P)	Negative (N)
Positive (P)	True Positive (TP)	False Negative (FN)
Negative (N)	False Positive (FP)	True Negative (TN)

TP is the correctly predicted part of the positives. FP is normally negative, but it is the part that is incorrectly predicted by the machine learning algorithm and thought to be positive. FN is the part that is normally positive but is incorrectly predicted by the machine learning algorithm and thought to be negative. TN is negative and is the part that the machine learning algorithm predicted correctly. Positive(P) is the sum of TP and FN. Negative(N) is the sum of FP and TN. Using all these values, it is calculated how successful the machine learning algorithm is. As a result of these calculations, the system's values such as accuracy (ACC), sensitivity (SEN), specificity (SPE), false discovery rate (FDR), and precision (PRE) are learned.

When calculating ACC, TP and TN are added and the result is divided by the sum of P and N. Other known names for sensitivity are recall, hit rate, or true positive rate. When calculating SEN, TP is divided by P. Specificity can also be called selectivity or true negative rate. When calculating SPE, TN is divided by N. When calculating FDR, FP is divided by the sum of FN and TN. Precision is also known as positive predictive value. When calculating PRE, TP is divided by the sum of TP and FP.

In this thesis study, TP is correctly defined as ADHD patients. TN represents the number of correctly identified healthy people. FP represents healthy people who are misidentified. FN represents the number of misidentified ADHD patients.

4.2 CNN Architectures

Designed CNN architectures and ResNet50 are included in this section.

4.2.1 Design1

First of all, the Dataset is divided into 70% train, 15% test, 15% validation. Input shape is 64 x 64 x 3. These pictures are the same size as their resized version. This designed 2D-CNN architecture is referred to as Design1 in this thesis study. In Design1, the convolutional layer comes first. As in Table 3, Layer parameters are (32, (3, 3)). ReLU is used as the activation function. Then comes the pooling process in 2x2 size. After this process, the convolutional layer comes again. In this study, ReLU was used as the activation function in all intermediate layers. After the pooling process, a convolutional layer comes again. The dimensions of the pooling operation are all (2, 2). The size of the convolutional layer is (64, (3, 3)). After this process, Flatten comes and then Dense comes in size 64. The activation function is ReLU. Finally, since there are 2 classes, there is a layer. Sigmoid was used as the activation function. Then there are the arguments of the model. These arguments are optimizer, loss, metrics, and learning rate. Kerasin's default values are used for other arguments. In this architecture the optimizer is Adam. Loss is binary_crossentropy. Accuracy is used for metrics. The default value of 0.001 was used for the learning rate. The reason for this is that the highest accuracy was achieved with these values. Also, the number of epochs is 10. batch size is 16. Figure 26 shows the block diagram of Design1.

Table 3. Summary of Design1 architecture.

Type	Layer Parameters	Output Size	Param	Activation
Conv2D	(32, (3, 3))	(None,62,62,32)	896	ReLU
MaxPooling2D	(2, 2)	(None, 31, 31, 32)	0	
Conv2D	(64, (3,3))	(None, 29, 29, 64)	18496	ReLU
MaxPooling2D	(2, 2)	(None, 14, 14, 64)	0	
Conv2D	(64, (3, 3)	(None, 12, 12, 64)	36928	ReLU
Flatten		(None, 512)	0	
Dense	64	(None, 64)	589888	ReLU
Dense	1	(None,1)	65	Sigmoid
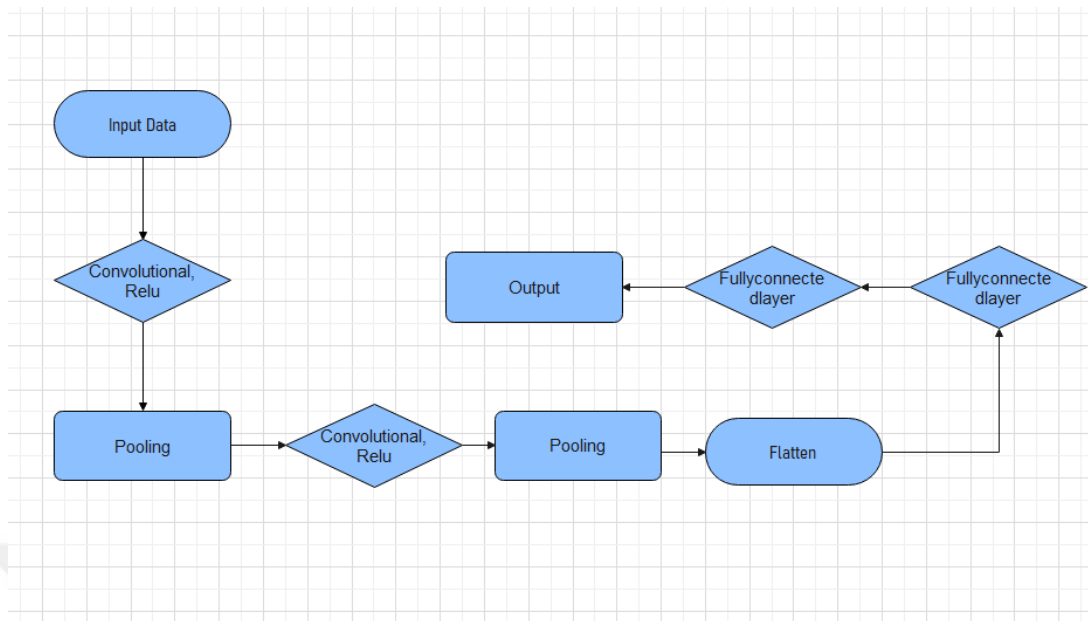
Figure 26. Block diagram of the Design1

4.2.2 Design2

First of all, this 2nd designed 2D-CNN architecture is named Design2. As in Dataset Design1, it is divided into 70% train, 15% test, and 15% validation. Input shape is 64 x 64 x 3. In Design2, the convolutional layer comes first. Layer parameters are (32, (3, 3)). Relu is used as the activation function. Then comes the pooling process in 2x2 size. Then the convolutional layer comes again and its size is (64, (3, 3)). After this process, pooling comes again. The size is 2 x 2 like previous pooling. After this process, the convolutional layer comes and its size is (128, (3, 3)). Then, the pooling process is redone. The size of the pooling used in this CNN architecture is 2 x 2. After pooling, the convolutional layer comes again and its size is (256, (3, 3)). After the convolutional layer, the pooling process comes. After Pooling, there is the Flatten operation. After the Flatten operation, there come Dense layers. Its size is 512 and its activation function is ReLU. After Dense layers, there comes the Dropout operation, by doing so, half of the issued units are the Dropout operation. After the Dropout operation, there come Dense layers. Its size is 256 and its activation function is ReLU. After Dense layers, the Dropout operation is redone. The Dropout operation parameter is 0.3. Finally, since there are 2 classes, there is one last Dense layer with one layer.

35

Sigmoid was used as the activation function. Then, there are the arguments of the model. These arguments are optimizer, loss, metrics, and learning rate. Keras' default values are used for other arguments. In this architecture, the optimizer is Adam. Loss is binary_crossentropy. Accuracy is used for metrics. The default value of 0.001 was used for the learning rate. The reason for this is that the highest accuracy was achieved with these values. Also, the number of epochs is 10, and batch size is 16. The architectural summary of Design2 is as in Table 4. The block diagram of Design2 is shown in Figure 27.

Table 4. Summary of Design2 architecture.

Type	Layer Parameters	Output Size	Param	Activation
Conv2D	(32, (3, 3))	(None,62,62,32)	896	ReLU
MaxPooling2D	(2, 2)	(None, 31, 31, 32)	0	
Conv2D	(64,(3,3))	(None, 31, 31, 32)	18496	ReLU
MaxPooling2D	(2, 2)	(None, 14, 14, 64)	0	
Conv2D	(128, (3, 3)	(None, 12, 12, 128)	73856	ReLU
MaxPooling2D	(2, 2)	(None, 6, 6, 128)	0	
Conv2D	(256, (3, 3)	(None, 4, 4, 256)	295168	ReLU
MaxPooling2D	(2, 2)	(None, 2, 2, 256)	0	
Flatten		(None, 1024)	0	
Dense	512	(None, 512)	524800	ReLU
Dropout	0.5	(None, 512)	0	
Dense	256	(None, 256)	131328	ReLU
Dropout	0.3	(None, 256)	0	
Dense	1	(None,1)	257	Sigmoid
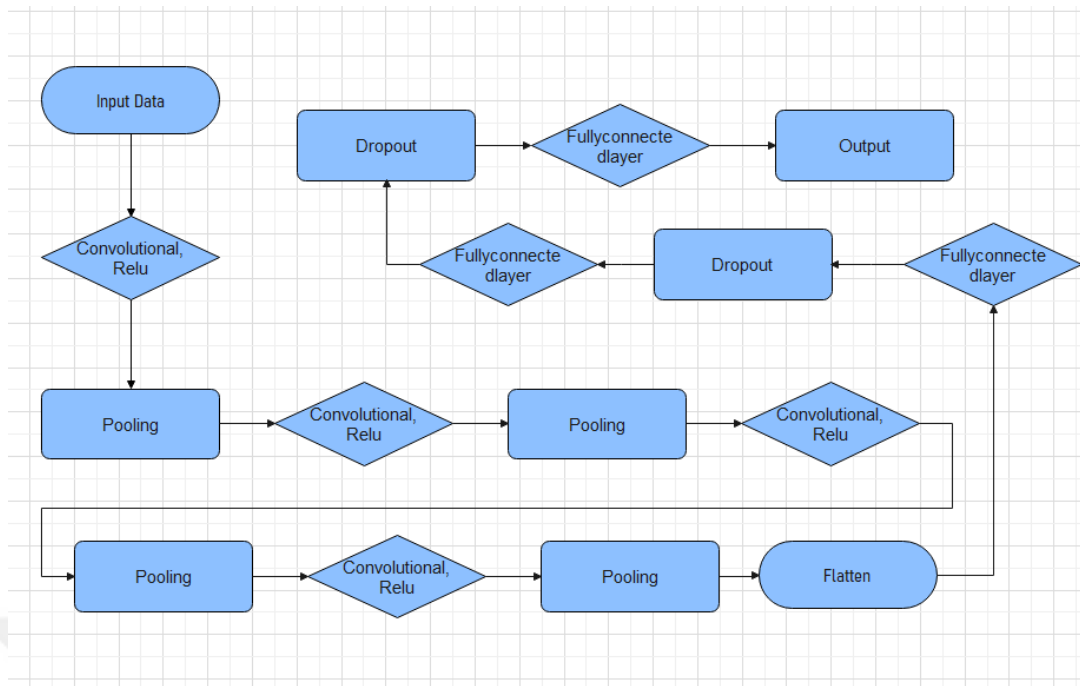
Figure 27. Block diagram of the Design2

4.2.3 ResNet-50

ResNet-50 is a pre-trained neural network. It is a CNN architecture. In this study, ResNet-50 was used in the Matlab environment. The input values of the original version are 224 x 224 x 3. Therefore, the input layer was changed in this study. Additionally, the size values are made 64 x 64 x 3. Since ResNet-50 has 1000 classes in its original form, the output size in the fully connected layer is 1000. Since there are 2 classes in this study, the output size of the fullyconnectedlayer is changed to 2. The last layer of ResNet-50 is the ClassificationLayer. The output size of this is 1000. In this study, the output size was changed to auto. Other values and parameters of ResNet-50 are used in their original form. ResNet-50's training options are as shown in Figure 28.

Figure 28. Training options of ResNet-50

4.3 2D-CNN Results with the IMFs in All Regions

In this thesis study, TP is correctly defined for ADHD patients. TN represents the number of correctly identified healthy people. FP represents healthy people who are misidentified. FN represents the number of misidentified ADHD patients.

In this part of the study, there are classification results with 3 different CNN architectures. These are IMFs obtained with the help of the EMD function as input. The first 5 IMFs were used in this thesis. Also, The first 3 IMFs are given as input in different combinations used in this thesis. The results are given in Table 5 and Table 6.

Table 5. Results of IMFs in all regions

CNN Model	IMF	Learning Rate	Validation Accuracy	Sensitivity	Precision	F1 Score
Design1	IMF1	0.001	0.81185	0.78413	0.79087	0.78748
Design1	IMF2	0.001	0.76819	0.68105	0.77082	0.72317
Design1	IMF3	0.001	0.74318	0.75343	0.69471	0.72289
Design1	IMF4	0.001	0.68276	0.51810	0.69100	0.59219
Design1	IMF5	0.001	0.67288	0.59166	0.64373	0.61660
Design2	IMF1	0.001	0.76913	0.65917	0.78694	0.71745
Design2	IMF2	0.001	0.76751	0.81788	0.70586	0.75775
Design2	IMF3	0.001	0.74210	0.70964	0.71007	0.70986
Design2	IMF4	0.001	0.70235	0.55487	0.71205	0.62371
Design2	IMF5	0.001	0.69329	0.46579	0.74951	0.57453
ResNet-50	IMF1	0.001	0.82387	0.79315	0.80690	0.79996
ResNet-50	IMF1	0.010	0.84995	0.84231	0.82375	0.83293
ResNet-50	IMF1	0.100	0.76345	0.88097	0.68046	0.76641
ResNet-50	IMF2	0.001	0.75810	0.68538	0.73735	0.71042
ResNet-50	IMF2	0.010	0.78366	0.74718	0.76120	0.75412
ResNet-50	IMF2	0.100	0.75811	0.68812	0.74714	0.71642
ResNet-50	IMF3	0.001	0.75540	0.71537	0.72879	0.72202
ResNet-50	IMF3	0.010	0.77994	0.73378	0.76185	0.74755
ResNet-50	IMF3	0.100	0.76399	0.82815	0.69720	0.75706
ResNet-50	IMF4	0.001	0.66822	0.62039	0.62794	0.62414
ResNet-50	IMF4	0.010	0.68396	0.63729	0.64614	0.64168
ResNet-50	IMF4	0.100	0.70417	0.55844	0.71311	0.62637
ResNet-50	IMF5	0.001	0.66524	0.57899	0.63495	0.60568
ResNet-50	IMF5	0.010	0.69386	0.61019	0.67062	0.63898
ResNet-50	IMF5	0.100	0.70640	0.57305	0.70984	0.63415

As in Table 5, the highest Validation Accuracy obtained for Design1 is 0.81185. This result is achieved with IMF1 as the input.

Considering these results, the prediction rate of healthy people is higher than the prediction rate of sick people. That's why sensitivity and precision values are lower than Validation Accuracy. Sensitivity values are very important in this study. Because mistakenly classifying a sick person as healthy can be life-threatening. In this study, FP values were tried to be reduced as much as possible. The most successful results were obtained for Design1 when the input was IMF1. There is no big difference

between Validation Accuracy values when the input for Design1 is IMF2 and IMF3. But there is a huge difference between Sensitivity results. When the input is IMF2, the Validation Accuracy value is slightly higher than the value when the input is IMF3. However, when the input is IMF3, the Sensitivity value is much higher than the value when the input is IMF2. When looking at the Validation Accuracy for Design1, it can be seen that IMF2 was more successful than IMF3. However, when looking at Sensitivity, the situation is exactly the opposite. If there is not a big difference between Validation Accuracies, it makes sense to look at Sensitivity to interpret which system is more successful. For Design1, IMF3 is better than IMF2. It cannot be said that the system is successful for IMF4 and IMF5. Especially when looking at the Sensitivity value of IMF4, it is seen that it was very close to 50%. The worst rate for a machine learning algorithm is 50%. For example, a rate of 10% is a successful rate, and by taking it inversely, a rate of 90% is reached. At rates of 50% and close to 50%, it is concluded that the system cannot classify. When classifying ADHD, the first three IMFs gave better results when Design1 was used.

Design 2 used more layers than Design1. When the results of Design2 were analyzed, it can be seen that results almost similar to the results of Design 1 were obtained. However, when IMF1 is taken as input, Design1 is better than Design2. The IMF2 classification for Design2 has been the most successful. Because, although the Validation Accuracy values are close for the first 3 IMFs, the sensitivity value of IMF2 increases perceptibly. That's why IMF2 achieved the best result in classification. There is no big difference between IMF3 and IMF1. IMF4 and IMF5 also fail as in Design1. When you look at the validation accuracy in Design2, the order of success is IMF1, IMF2, IMF3, IMF4, and IMF5 respectively. According to sensitivity values, the most successful input was IMF2. The order of success is IMF3, IMF1, IMF4, and IMF5 respectively. For IMF5, by subtracting the sensitivity values of 0.46579 from 1, the value of 0.53421 is reached. The sensitivity value of IMF5 can be said to be 0.53421.

When IMFs are given in different combinations as input, as in Table 6, the accuracy rate decreases. In this table, the highest accuracy was obtained in Desing1 when IMF1 and IMF2 were given together. When IMF1 and IMF3 were given together for Design2, the highest Accuracy rate was obtained for Design2. When IMF1, IMF2, and IMF3 were given together, Desing1 was more successful than Desing2.

Table 6. The first 3 IMFs are used as input with different combinations.

CNN Model	Input	Validation Accuracy	Sensitivity	Precision	F1 Score
Design1	IMF1, IMF2	0.78859	0.63210	0.85450	0.72666
Design1	IMF1, IMF3	0.56001	0.0	0.0	0.0
Design1	IMF2, IMF3	0.56001	0.0	0.0	0.0
Design1	IMF1, IMF2, IMF3	0.70379	0.64434	0.67778	0.66064
Design2	IMF1, IMF2	0.56001	0.0	0.0	0.0
Design2	IMF1, IMF3	0.74763	0.64331	0.74785	0.69165
Design2	IMF2, IMF3	0.56001	0.0	0.0	0.0
Design2	IMF1, IMF2, IMF3	0.66342	0.79830	0.59186	0.67975

4.4 2D-CNN Results with the IMFs in Right Temporal Regions

This section contains the results in the Right Temporal region. In regional studies, only Design1 and Design2 were tested. ResNet-50 is not used in this section.

The results in the Right Temporal and Anterior regions have a higher accuracy than the results in other regions. Looking at the results in the Right Temporal region, Design2 was slightly more successful than Design1, as shown in Table 7. Considering these results, the use of more layers and the use of extra pooling and Dropout increased Accuracy. When the sensitivity values are examined, the highest value is reached when the input is IMF3. In this case, IMF3 was more successful in classifying the Control dataset. When looking at Validation Accuracy, the order of success for Design2 is IMF1, IMF2, IMF3, IMF4, and IMF5. The order of success for Design1 is IMF1, IMF2, IMF3, IMF5, and IMF4. When the input is IMF2, the Sensitivity value for Design1 is the same as IMF3. The Validation Accuracy value is approximately 0.02 percent higher. In this case, IMF2 is slightly more successful than IMF3. For Design2, the highest Sensitivity value was reached with IMF3. However, the highest Validation Accuracy value is with IMF1. Considering all the results, the first three IMFs are more successful.

Table 7. Results in the Right Temporal region

CNN Model	IMF	Learning Rate	Validation Accuracy	Sensitivity	Precision	F1 Score
Design1	IMF1	0.001	0.79107	0.63103	0.85139	0.72751
Design1	IMF2	0.001	0.78093	0.73210	0.76019	0.74588
Design1	IMF3	0.001	0.76876	0.73210	0.73892	0.73549
Design1	IMF4	0.001	0.69979	0.67436	0.65324	0.66363
Design1	IMF5	0.001	0.72413	0.62124	0.71352	0.66419
Design2	IMF1	0.001	0.81541	0.68822	0.86376	0.76606
Design2	IMF2	0.001	0.81135	0.79676	0.77878	0.78767
Design2	IMF3	0.001	0.76572	0.82217	0.69803	0.75503
Design2	IMF4	0.001	0.72718	0.74133	0.67154	0.70472
Design2	IMF5	0.001	0.67545	0.76212	0.60329	0.67346

4.5 2D-CNN Results with the IMFs in Cental Regions

This section contains the results in the Cental region. In regional studies, only Design1 and Design2 were tested. ResNet50 is not used in this section. The highest Sensitivity value was obtained with IMF1 for Design1 in the Cental region. The same situation applies to Design2. Therefore, when IMF1 is used as the input, the most decisive region for the Control dataset is the Cental region. In Validation Accuracy, using Design2, the highest value is in the Cental region. It has almost the same Validation Accuracy value as the value with IMF1 in the Right Temporal Region. Other results in the central region are also decent. The values of Design2 are better than Design1. Therefore, the extra layer, pooling, and dropout sections were decisive for the Central region. As in other parts, the first three IMFs have higher Accuracy. The results in the Cental region are as in Table 8.

Table 8. Results in the Cental region

CNN Model	IMF	Learning Rate	Validation Accuracy	Sensitivity	Precision	F1 Score
Design1	IMF1	0.001	0.77972	0.83493	0.70026	0.76169
Design1	IMF2	0.001	0.77770	0.67948	0.76672	0.72042
Design1	IMF3	0.001	0.74256	0.73237	0.68107	0.70579
Design1	IMF4	0.001	0.67229	0.63942	0.60546	0.62197
Design1	IMF5	0.001	0.69594	0.68910	0.62682	0.65658
Design2	IMF1	0.001	0.81486	0.78685	0.77689	0.78184
Design2	IMF2	0.001	0.80769	0.80769	0.74777	0.77657
Design2	IMF3	0.001	0.76081	0.70352	0.72203	0.71266
Design2	IMF4	0.001	0.68986	0.64583	0.62870	0.63715
Design2	IMF5	0.001	0.69324	0.61538	0.64214	0.62847

4.6 2D-CNN Results with the IMFs in Anterior Regions

This section contains the results in the Anterior Region. In regional studies, only Design1 and Design2 were tested. ResNet50 is not used in this section. When the input for Design1 was IMF1, the highest Validation Accuracy value was reached in the Anterior Region. When the input was IMF1, IMF2, and IMF5; the Design1 Validation Accuracy value was higher than Design2. Therefore, the extra layer, pooling, and dropout parts reduced the accuracy for the Anterior region. It has relatively lower values than the Right Temporal Region and the Cental Region. They have higher Validation Accuracy values than the Posterior Region and the Left Temporal Region. As in other regions, the Validation Accuracy of the first 3 IMFs is much higher than the last 2 IMFs. The results in the Anterior region are as in Table 9.

Table 9. Results in the Anterior region

CNN Model	IMF	Learning Rate	Validation Accuracy	Sensitivity	Precision	F1 Score
Design1	IMF1	0.001	0.79669	0.78303	0.76199	0.77237
Design1	IMF2	0.001	0.77230	0.76712	0.71519	0.74025
Design1	IMF3	0.001	0.71031	0.64383	0.66197	0.65277
Design1	IMF4	0.001	0.66628	0.58767	0.60937	0.59832
Design1	IMF5	0.001	0.67786	0.56712	0.63302	0.59826
Design2	IMF1	0.001	0.77636	0.69041	0.75903	0.72309
Design2	IMF2	0.001	0.74971	0.78493	0.67570	0.72623
Design2	IMF3	0.001	0.76940	0.69315	0.74411	0.71773
Design2	IMF4	0.001	0.69988	0.55068	0.67905	0.60816
Design2	IMF5	0.001	0.66628	0.69315	0.58974	0.63727

4.7 2D-CNN Results with the IMFs in Posterior Regions

This section contains the results in the Posterior Region. In regional studies, only Design1 and Design2 were tested. ResNet50 is not used in this section. The Posterior Region has lower Validation Accuracy than the Cental Region, the Anterior Region, and the Right Temporal Region. However, it has higher Validation Accuracy than the Left Temporal Region. There is almost no difference between Validation or Sensitivity values for Design1 and Design2. Therefore, the extra layer, pooling, and dropout sections did not have much effect on accuracy. 2D-CNN with fewer layers can be used for classification. As in other regions, the accuracy of the first three IMFs is higher. The last two IMFs are lower in accuracy. Although the Posterior Region is not very good for ADHD classification, it can be classified at an average level. The results in

the Posterior region are as in Table 10.

Table 10. Results in the Posterior region

CNN Model	IMF	Learning Rate	Validation Accuracy	Sensitivity	Precision	F1 Score
Design1	IMF1	0.001	0.74222	0.72945	0.70679	0.71794
Design1	IMF2	0.001	0.70301	0.69238	0.66251	0.67711
Design1	IMF3	0.001	0.72149	0.73146	0.67592	0.70259
Design1	IMF4	0.001	0.65164	0.63126	0.60869	0.61977
Design1	IMF5	0.001	0.67282	0.59819	0.64750	0.62187
Design2	IMF1	0.001	0.74673	0.70741	0.72336	0.71529
Design2	IMF2	0.001	0.73366	0.66132	0.72289	0.69073
Design2	IMF3	0.001	0.70166	0.71643	0.65564	0.68355
Design2	IMF4	0.001	0.67237	0.60621	0.64430	0.62467
Design2	IMF5	0.001	0.65209	0.63927	0.60761	0.62304

4.8 2D-CNN Results with the IMFs in the Left Temporal Region

This section contains the results in the Left Temporal Region. In regional studies, only Design1 and Design2 were tested. ResNet50 is not used in this section. The Left Temporal Region has the lowest Validation Accuracy compared to other regions. The classification success rate for ADHD is low with data from this field. In particular, no classification could be made for IMF5. When Design1 and Design2 were compared in the classification made in this region, Design2 was more successful than Design1. Therefore, the extra layer, pooling, and dropout sections had a great impact on accuracy. In the case of classification for data taken from the Left Temporal Area, a more complex CNN needs to be designed. As in Table 10, the most interesting ratio is the ratio with Design2 and IMF3 as its input. This rate is the highest compared to other regions. Although it is less successful with other inputs, it has the most successful classification for IMF3 in the Left Temporal region. Especially when a complex CNN is designed and the input is IMF3 with the correct parameter values, the success rate is going to increase. The results in the Left Temporal region are as in Table 11.

Table 11. Results of CNN models in the Left Temporal region with IMFs

CNN Model	IMF	Learning Rate	Validation Accuracy	Sensitivity	Precision	F1 Score
Design1	IMF1	0.001	0.67139	0.59815	0.63325	0.61520
Design1	IMF2	0.001	0.68965	0.58891	0.66579	0.62500
Design1	IMF3	0.001	0.68356	0.61893	0.64578	0.63207
Design1	IMF4	0.001	0.65314	0.56581	0.61403	0.58894
Design1	IMF5	0.001	0.56085	0.00000	0.00000	0.00000
Design2	IMF1	0.001	0.73022	0.59815	0.73789	0.66071
Design2	IMF2	0.001	0.71196	0.54272	0.73208	0.62334
Design2	IMF3	0.001	0.77079	0.70438	0.75682	0.72966
Design2	IMF4	0.001	0.67951	0.66974	0.62634	0.64732
Design2	IMF5	0.001	0.56085	0.00000	0.00000	0.00000

4.9 2D-CNN Results with EEG Signal

In this section, classification was made in the data set by taking the spectrogram of the EEG signal. There is no big difference between Validation Accuracies when Design1 and Design2 are used, both have a success rate of over 90%. Design1 is slightly better than Design2 in classification. ResNet-50 has been the most successful in its operations in this classification. It has the highest validation accuracy when the learning rate is 0.01. This type of order of success continues with 0.1 and 0.001 as the learning rate. Since all Validation accuracy rates are above 92%, all Learning Rate values are successful. If preferred, 0.01 would give the best result because the Sensitivity rate came out to be 96.742% and the Accuracy rate was 96.526%. The accuracy rates in this section are close to the rates in other ADHD classifications studied in the literature. As in Table 12, ResNet-50 gave the highest Accuracy rate of 96.526%, especially when the learning rate was 0.01. When compared to other studies on the ADHD data set in Table 13, almost the best Accuracy rate was achieved.

When viewed regionally, the highest accuracy rate for Design1 belongs to the Posterior Region. After the Posterior Region, the region with the highest accuracy is the Cental Region. Following this, the highest accuracy rate belongs to the Anterior Region. Next comes the Left Temporal Region accuracy rate. Finally, the region with the lowest accuracy rate is the Right Temporal Region.

This order is different for Design2. The Anterior Region has the most succes rate. The Right Temporal Region comes second. It has the lowest accuracy rate for Design1. In

this case, designing a more complex CNN for the Right Temporal Region increases the accuracy rate. The Cental Region comes third. The Left Temporal Region comes fourth. Finally, the least successful region is the Posterior Region. In this case, it is necessary to design a simpler CNN when classifying with data from the Posterior Region.

Considering all these situations, the reason for the lower accuracy rate in regional classification is that there is less data. In this case, data augmentation is recommended to increase the data in regional studies. Over 96% accuracy was achieved in all experiments in this section. This is a quite successful situation for ADHD classification.

Table 12. Results of CNN models with EEG signal

CNN Model	Region	Learning Rate	Validation Accuracy	Sensitivity	Precision	F1 Score
Design1	All	0.001	0.91916	0.93675	0.88764	0.91153
Design2	All	0.001	0.90565	0.91638	0.87692	0.89622
ResNet-50	All	0.001	0.92160	0.93471	0.93508	0.93891
ResNet-50	All	0.01	0.96526	0.96742	0.95492	0.96113
ResNet-50	All	0.1	0.94430	0.95371	0.92362	0.93828
Design1	Posterior Region	0.001	0.90179	0.91505	0.88869	0.90169
Design2	Posterior Region	0.001	0.86983	0.81859	0.91908	0.86618
Design1	Cental Region	0.001	0.88783	0.88177	0.89256	0.88714
Design2	Cental Region	0.001	0.89633	0.91260	0.88062	0.89634
Design1	Left Temporal Region	0.001	0.88269	0.86843	0.89537	0.88171
Design2	Left Temporal Region	0.001	0.87814	0.88869	0.86774	0.87810
Design1	Anterior Region	0.001	0.88619	0.86831	0.90251	0.88511
Design2	Anterior Region	0.001	0.91011	0.90628	0.91362	0.90994
Design1	Right Temporal Region	0.001	0.82991	0.91447	0.76905	0.83603
Design2	Right Temporal Region	0.001	0.90362	0.91631	0.89127	0.90363

Table 13. Comparison between the accuracy of this method with some state-of-the-art studies in this area.

Work	Year	Participants	Accuracy (%)
Bakhtyari and Mirzaei	2022	46 ADHD/45 CS	99.75
Johnstone et al.	2021	53 ADHD/161 CS	81.20
Ghaderyan and et al.	2022	14 ADHD/19 CS	99.17
Altınkaynak et al.	2020	23 ADHD/23 CS	91.30
Güney et al.	2021	27 ADHD/38 CS	98.40
Vahid et al.	2019	100 ADHD/44 CS	83.00
Dubreuil-Vall, Ruffini and Camprodon	2020	20 ADHD/20 CS	88.00
Ahmadi et al.	2021	25 ADHD/14 CS	99.46
Moghaddari, Lighvan and Danishvar	2020	30 ADHD/31 CS	99.06
Chen et al.	2019	50 ADHD/58 CS	84.59
Rezaeezadeh, Shamekhi and Shamsi	2020	12 ADHD/12 CS	99.58
Khoshnoud Nazari and Shamsi	2018	12 ADHD/12 CS	83.33
Boroujeni, Rastegari and Khodadadi	2019	50 ADHD/26 CS	96.05
Yaghoobi Karimu and Azadi	2018	20 ADHD/20 CS	98.07
Cura, Atli and Akan	2023	15 ADHD/18 CS	99.06
Akan et al	2022	15 ADHD/18 CS	91.01
Akan et al	2023	15 ADHD/18 CS	99.75
This study	2023	15 ADHD/18 CS	96.53

CHAPTER 5: CONCLUSION and DISCUSSION

Early diagnosis is very important to improve the life standards of ADHD patients and to reduce future problems. In this thesis study, a deep learning model with EMD was designed for accurate classification. The classification was made with the IMFs obtained from the EMD function. Also, classification was made with the original signal. When the classification was made by using IMFs, an accuracy value of almost 85 percent was reached at most. Almost 97% accuracy value was reached in the classification process made with EEG signal. This rate is much higher than what could be achieved with the IMFs. In addition, it is close to other ADHD classification studies in literature or has a higher accuracy percentage than them. The reason why this is higher than IMFs is that the original signal contains more information than IMFs when the spectrogram is taken. Therefore, 2D-CNN was more successful in classification. To increase the success rate of classification with IMFs, CNN's parameter values can be selected in a more optimized way. Additionally, the first three IMFs can be combined and turned into a volume and classified with 3D-CNN. By doing so, the amount of data can be increased, and a more successful classification can be achieved. Additionally, accuracy can be increased with data augmentation methods. For good measure, other advanced signal processing techniques other than EMD can be used. For example, the intrinsic time-scale decomposition (ITD) is an option. The results obtained are comparable to EMD. Also, derivatives of EMD, the Ensemble Empirical Mode Decomposition (EEMD), and the Multivariate Empirical Mode Decomposition (MEMD) are appropriate alternatives. The results obtained can be compared with EMD. Combining the results of all these, the best advanced signal processing technique for ADHD classification can be accomplished. Most importantly, more powerful hardware is a must to work with larger datasets.

REFERENCES

Ahmadi, A., Kashefi, M., Shahrokhi, H. and Nazari, M. A. (2021) *Computer aided diagnosis system using deep convolutional neural networks for ADHD subtypes*. Biomedical Signal Processing and Control, Vol. 63, p. 102227.

Akan, A. and Cura, O. K. (2021) *Analysis of epileptic EEG signals by using dynamic mode decomposition and spectrum.* Biocybernetics and Biomedical Engineering, Vol. 41(1), pp. 28-44.

Akbugday, B., Bozbas, O. A., Cura, O. K., Pehlivan, S. and Akan, A. (2023) *Detection of Attention Deficit Hyperactivity Disorder by Using EEG Feature Maps and Deep Learning*. In 2023 31st European Signal Processing Conference (EUSIPCO), pp. 1105-1109

Altınkaynak, M., Dolu, N., Güven, A., Pektaş, F., Özmen, S., Demirci, E. and İzzetoğlu, M. (2020). *Diagnosis of Attention Deficit Hyperactivity Disorder with combined time and frequency features*. Biocybernetics and Biomedical Engineering, Vol. 40(3), pp. 927-937.

Albawi, S., Mohammed, T. A. and Al-Zawi, S. (2017) *Understanding of a convolutional neural network.* In 2017 international conference on engineering and technology (ICET), pp. 1-6

Amado-Caballero, P., Casaseca-de-la-Higuera, P., Alberola-López, S., Andrés-de-Llano, J. M., López-Villalobos, J. A. and Alberola-López, C. (2023) *Insight into ADHD diagnosis with deep learning on Actimetry: Quantitative interpretation of occlusion maps in age and gender subgroups*. Artificial Intelligence in Medicine, Vol. 143, p. 102630.

Andreasen, S. M., Frederiksen, H., Bilenberg, N., Andersson, A. M., Juul, A., Kyhl, H. B. and Jensen, T. K. (2023) *Maternal concentrations of phthalates and Attention-Deficit Hyperactivity Disorder (ADHD-) related symptoms in children aged 2 to 4 years from Odense child cohort*. Environment International, Vol. 180, p. 108244.

Bakhtyari, M. and Mirzaei, S. (2022) *ADHD detection using dynamic connectivity patterns of EEG data and ConvLSTM with attention framework*. Biomedical Signal

Processing and Control, *Detection of Attention Deficit Hyperactivity Disorder by Using EEG Feature Maps and Deep Learnin*g Vol. 76, p. 103708.

Boroujeni, Y. K., Rastegari, A. A. and Khodadadi, H. (2019) *Diagnosis of attention deficit hyperactivity disorder using non-linear analysis of the EEG signal*. IET systems biology, Vol. 13(5), pp. 260-266.

Chen, H., Chen, W., Song, Y., Sun, L. and Li, X. (2019) *EEG characteristics of children with attention-deficit/hyperactivity disorder*. Neuroscience, Vol. 406, pp. 444-456.

Cura, O. K., Atli, S. K. and Akan, A. (2023) *Attention deficit hyperactivity disorder recognition based on intrinsic time-scale decomposition of EEG signals*. Biomedical Signal Processing and Control, Vol. 81, p. 104512.

Cura, O. K., Atli, S. K., Sen, S. Y. and Akan, A. (2023) *Classification of ADHD by Using Multiple Feature Maps of EEG Signals and Deep Feature Extraction.* In 2023 31st European Signal Processing Conference (EUSIPCO), pp. 1065-1069.

Cura, O. K., Aydin, G. N., Celen, S., Atli, S. K. and Akan, A. (2022) *Detection of Attention Deficit Hyperactivity Disorder Using EEG Signals and Douglas—Peucker Algorithm*. In 2022 Medical Technologies Congress (TIPTEKNO), pp. 1-4

Dauwels, J., Vialatte, F., Musha, T. and Cichocki, A. (2010) *A comparative study of synchrony measures for the early diagnosis of Alzheimer's disease based on EEG*. NeuroImage, Vol 49(1), pp. 668-693.

Degirmenci, M., Ozdemir, M. A., Izci, E. and Akan, A. (2022). *Arrhythmic heartbeat classification using 2d convolutional neural networks*. Irbm, Vol 43, pp. 422-433.

Do, D., Lee, T., Bably, M., Inneh, I. A. and Patel, U. (2023) *Prevalence and Predictors of Multimodal Treatment Among US Adults Newly Diagnosed With ADHD*. American Journal of Preventive Medicine.

Dubreuil-Vall, L., Ruffini, G. and Camprodon, J. A. (2020) *Deep learning convolutional neural networks discriminate adult ADHD from healthy individuals on the basis of event-related spectral EEG*. Frontiers in neuroscience, Vol. 14, p. 251.

Eid, D. (2023) *Parts Of the Brain: Anatomy, Structure & Functions.* [Online]. Available at: https://www.simplypsychology.org/forebrain-midbrain-hindbrain.html. (Accessed: 17 August 2023)

Ghaderyan, P., Moghaddam, F., Khoshnoud, S. and Shamsi, M. (2022) *New interdependence feature of eeg signals as a biomarker of timing deficits evaluated in attention-deficit/hyperactivity disorder detection.* Measurement, Vol. 199, p. 111468.

Güney, G., Kisacik, E., Kalaycıoğlu, C. and Saygili, G. (2021) *Exploring the attention process differentiation of attention deficit hyperactivity disorder (ADHD) symptomatic adults using artificial intelligence onelectroencephalography (EEG) signals.* Turkish Journal of Electrical Engineering and Computer Sciences, Vol. 29(5), pp. 2312-2325.

Huang, N. E., Shen, Z., Long, S. R., Wu, M. C., Shih, H. H., Zheng, Q., Yen, N. C. Tung, C. C. and Liu, H. H. (1998) *The empirical mode decomposition and the Hilbert spectrum for nonlinear and non-stationary time series analysis.* Proceedings of the Royal Society of London. Series A: mathematical, physical and engineering sciences, Vol. 454(1971), pp. 903-995.

Johnstone, S. J., Parrish, L., Jiang, H., Zhang, D. W., Williams, V. and Li, S. (2021) *Aiding diagnosis of childhood attention-deficit/hyperactivity disorder of the inattentive presentation: Discriminant function analysis of multi-domain measures including EEG.* Biological Psychology, Vol. 161, pp. 108080.

Kenter, R. M. F., Lundervold, A. J. and Nordgreen, T. (2021) *A self-guided internet-delivered intervention for adults with ADHD: a protocol for a randomized controlled trial.* Internet Interventions, Vol. 26, p. 100485.

Khoshnoud, S., Nazari, M. A. and Shamsi, M. (2018) *Functional brain dynamic analysis of ADHD and control children using nonlinear dynamical features of EEG signals.* Journal of integrative neuroscience, Vol. 17(1), pp. 17-30

Krizhevsky, A., Sutskever, I. and Hinton, G. E. (2017) *ImageNet classification with deep convolutional neural networks.* Communications of the ACM, Vol. 60(6), pp. 84-90

Lewis, J. W., Lama, A. M., Hogg, J. P., Boo, S., Tucker, E. S., Brown, C. M., Zdilla, M. J., Petrone, A., Lambert, H. W., Agmon, A., Billings, H., Roth, L., Patterson, B. and Palmer, B. (2023) *Online interactive medical neuroimaging exercise to identify*

human brain structures. Annals of Anatomy-Anatomischer Anzeiger, Vol. 249, p. 152101.

Locatelli, T., Cursi, M., Liberati, D., Franceschi, M. and Comi, G. (1998*) EEG coherence in Alzheimer's disease.* Electroencephalography and clinical neurophysiology, Vol. 106(3), pp. 229-237

Mao, Z., Su, Y., Xu, G., Wang, X., Huang, Y., Yue, W., Sun, L. and Xiong, N. (2019) *Spatio-temporal deep learning method for adhd fmri classification.* Information Sciences, Vol. 499, pp. 1-11.

Mert, A., and Akan, A. (2014) *Detrended fluctuation thresholding for empirical mode decomposition based denoising.* Digital signal processing, Vol. 32, pp. 48-56.

Mert, A. and Akan, A. (2018) *Seizure onset detection based on frequency domain metric of empirical mode decomposition*. Signal, Image and Video Processing, Vol. 12, pp. 1489-1496.

Moghaddari, M., Lighvan, M. Z. and Danishvar, S. (2020) *Diagnose ADHD disorder in children using convolutional neural network based on continuous mental task EEG*. Computer Methods and Programs in Biomedicine, Vol. 197, p. 105738.

Oon, H. N., Saidatul, A. and Ibrahim, Z. (2018) *Analysis on Non-linear features of electroencephalogram (EEG) signal for neuromarketing application.* In 2018 international conference on computational approach in smart systems design and applications (ICASSDA), pp. 1-8

Rezaeezadeh, M., Shamekhi, S. and Shamsi, M. (2020) *Attention Deficit Hyperactivity Disorder Diagnosis using non-linear univariate and multivariate EEG measurements: a preliminary study*. Physical and engineering sciences in medicine, Vol. 43, pp. 577-592.

Srivastava, N., Hinton, G., Krizhevsky, A., Sutskever, I. and Salakhutdinov, R. (2014) *Dropout: a simple way to prevent neural networks from overfitting.* The journal of machine learning research, Vol. 15(1), pp. 1929-1958.

TaghiBeyglou, B., Shahbazi, A., Bagheri, F., Akbarian, S. and Jahed, M. (2022) *Detection of ADHD cases using CNN and classical classifiers of raw EEG*. Computer Methods and Programs in Biomedicine Update, Vol. 2, p. 100080.

Tor, H. T., Ooi, C. P., Lim-Ashworth, N. S., Wei, J. K. E., Jahmunah, V., Oh, S. L., Acharya, U. R. and Fung, D. S. S. (2021) *Automated detection of conduct disorder and attention deficit hyperactivity disorder using decomposition and nonlinear techniques with EEG signals.* Computer Methods and Programs in Biomedicine, Vol. 200, p. 105941.

Vahid, A., Bluschke, A., Roessner, V., Stober, S. and Beste, C. (2019) *Deep learning based on event-related EEG differentiates children with ADHD from healthy controls*. Journal of clinical medicine, Vol. 8(7), p. 1055.

Yaghoobi Karimu, R. and Azadi, S. (2018) *Diagnosing the ADHD using a mixture of expert fuzzy models.* International Journal of Fuzzy Systems, Vol. 20, pp. 1282-1296.

APPENDICES

Appendix A.

Algorithm 1: EMD

---

6. Local minima Lm_i, $i = 1, 2, ...$ and Local maxima Lx_j, $j = 1, 2, ...$ are found using input signal $x[n]$.

7. Calculate $Ue[n]$ and $Le[n]$ which upper and lower envelopes respectively, using cubic interpolation.
8. Mean of envelopes value is found.

9. Compute $d_1[n] = x[n] - Me[n]$. If $d_1[n]$ satisfies the condition of IMF,

$d_1[n] = IMF_1[n]$. Else go to step 1 and repeat every processes using $d_1[n]$ instead of $x[n]$.
10. After obtaining $IMF_1[n]$ calculate the residue $R_1[n] = x[n] - IMF_1[n]$. If this residue has more than a zero-cross, return step 1 and calculate again new IMF.

This process will continue until last residue $R_L[n]$ which has no zero cross is obtained and all necessary conditions are satisfied.

We can reconstruct the original signal $x[n]$ using the following formulation:

$$x[n] = \left(\sum_{l=1}^{L} IMF_l[n] \right) + R_L[n]$$

Here, L is the number of $IMFs$ and $R_L[n]$ is the residue.

Appendix B.

T.C.
İZMİR KÂTİP ÇELEBİ ÜNİVERSİTESİ
Klinik Araştırmalar Etik Kurulu Karar Formu

ARAŞTIRMANIN AÇIK ADI	DİKKAT EKSİKLİĞİ HİPERAKTİVİTE BOZUKLUĞU TANISI OLAN ÇOCUKLARDA SENSORİYEL VE SENSORİMOTOR PERDELEMENİN İNCELENMESİ
VARSA ARAŞTIRMANIN PROTOKOL KODU	

ETİK KURUL BİLGİLERİ	İTİK KURULUN ADI	İzmir Katip Çelebi Üniversitesi Tıp Fakültesi Klinik Araştırmalar Etik Kurulu
	AÇIK ADRESİ:	İzmir Katip Çelebi Üniversitesi Atatürk Eğitim Ve Araştırma Hastanesi 35360 Karabağlar/İZMİR
	TELEFON	0232 245 04 38
	FAKS	0232 245 04 38
	E-POSTA	-

BAŞVURU BİLGİLERİ	KOORDİNATÖR/SORUMLU ARAŞTIRMACI UNVANI/ADI/SOYADI	Dr. Öğr. Üyesi Gonca ÖZYURT			
	KOORDİNATÖR/SORUMLU ARAŞTIRMACININ UZMANLIK ALANI	Çocuk ve Ergenlik Ruh Sağlığı ve Hastalıkları			
	KOORDİNATÖR/SORUMLU ARAŞTIRMACININ BULUNDUĞU MERKEZ	İzmir Katip Çelebi Üniversitesi Tıp Fakültesi			
	VARSA İDARİ SORUMLU UNVANI/ADI/SOYADI	--			
	DESTEKLEYİCİ	--			
	PROJE YÜRÜTÜCÜSÜ UNVANI/ADI/SOYADI (TÜBİTAK vb. gibi kaynaklardan destek alınlar için)	--			
	DESTEKLEYİCİNİN YASAL TEMSİLCİSİ	--			
	ARAŞTIRMANIN FAZI VE TÜRÜ	FAZ 1	☐		
		FAZ 2	☐		
		FAZ 3	☐		
		FAZ 4	☐		
		Gözlemsel ilaç çalışması	☐		
		Tıbbi cihaz klinik araştırması	☐		
		In vitro tıbbi tanı cihazları ile yapılan performans değerlendirme çalışmaları	☐		
		İlaç dışı klinik araştırma	☒		
		Diğer ise belirtiniz			
	ARAŞTIRMAYA KATILAN MERKEZLER	TEK MERKEZ ☒	ÇOK MERKEZLİ ☐	ULUSAL ☒	ULUSLARARASI ☐

Appendix Figure B-1 The First Page of The Ethical Approval Form

1/3

56

...NIN AÇIK ADI	DİKKAT EKSİKLİĞİ HİPERAKTİVİTE BOZUKLUĞU TANISI OLAN ÇOCUKLARDA SENSORİYEL VE SENSORİMOTOR PERDELEMENİN İNCELENMESİ

VARSA ARAŞTIRMANIN PROTOKOL KODU

	Belge Adı	Tarihi	Versiyon Numarası	Dili
DEĞERLENDİRİLEN BELGELER	ARAŞTIRMA PROTOKOLÜ	27.05.2019		Türkçe ☒ İngilizce ☐ Diğer ☐
	BİLGİLENDİRİLMİŞ GÖNÜLLÜ OLUR FORMU	27.05.2019		Türkçe ☒ İngilizce ☐ Diğer ☐
	OLGU RAPOR FORMU	27.05.2019		Türkçe ☒ İngilizce ☐ Diğer ☐
	ARAŞTIRMA BROŞÜRÜ			Türkçe ☐ İngilizce ☐ Diğer ☐

	Belge Adı		Açıklama
DEĞERLENDİRİLEN DİĞER BELGELER	SİGORTA	☐	.
	ARAŞTIRMA BÜTÇESİ	☒ 24.01.2019	
	BİYOLOJİK MATERYEL TRANSFER FORMU	☐	.
	İLAN	☐	
	YILLIK BİLDİRİM	☐	
	SONUÇ RAPORU	☐	
	GÜVENLİLİK BİLDİRİMLERİ	☐	
	DİĞER:	☒	-Ön Başvuru Formu 27.05.2019 -Çocuklar İçin Bilgilendirilmiş Gönüllü Olur Formu 27.05.2019 -Gonca ÖZYURT (27.05.2019), Görsev YENER (27.05.2019), Sibel KOCAASLAN ALTI (27.05.2019), Mehmet Cemal KAHYA (27.05.2019) özgeçmiş formu -Çalışma akış şeması -Araştırma Ekibini İKU VE İLU Çerçevesinde Bilgilendirme Belgesi (imza tarihi 27.05.2019) -İlaç dışı klinik araştırma başvuru formu (imza tarihi 27.05.2019) -Dünya Tıp Helsinki Bildirgesi

	Karar No:76	Tarih:11.07.2019
KARAR BİLGİLERİ	Yukarıda bilgileri verilen başvuru dosyası ile ilgili 16.05.2019 tarihli etik kurul toplantısında istenen düzeltmeler araştırmacılar tarafından yapılmış uygun bulunmuş olup, çalışmanın başvuru dosyasında belirtilen merkezlerde gerçekleştirilmesinde etik ve bilimsel sakınca bulunmadığına toplantıya katılan etik kurul üyelerinin oy birliği ile karar verilmiştir. İlaç ve Biyolojik Ürünlerin Klinik Araştırmaları Hakkında Yönetmelik kapsamında yer alan araştırmalar/çalışmalar için Türkiye İlaç ve Tıbbi Cihaz Kurumu'ndan izin alınması gerekmektedir.	

İzmir Kâtip Çelebi Üniversitesi Klinik Araştırmalar Etik Kurulu	
ETİK KURULUN ÇALIŞMA ESASI	İlaç ve Biyolojik Ürünlerin Klinik Araştırmaları Hakkında Yönetmelik, İyi Klinik Uygulamaları Kılavuzu
BAŞKANIN UNVANI / ADI / SOYADI:	Doç. Dr. Barış KARADAŞ

Unvanı/Adı/Soyadı	Uzmanlık Alanı	Kurumu	Cinsiyet		Araştırma ile İlişki		Katılım *	
Doç. Dr. Barış KARADAŞ / Başkan	Tıbbi Farmakoloji	İKÇÜTF	E ☒	K ☐	E ☐	H ☒	E ☒	H ☐
Prof. Dr. Nihal OLGAÇ DÜNDAR / Başkan Yardımcısı	Çocuk Nörolojisi	İKÇÜTF	E ☐	K ☒	E ☐	H ☒	E ☒	H ☐
Prof. Dr. Servet AKAR	İç Hastalıkları/ Romatoloji	İKÇÜTF	E ☐	K ☒	E ☐	H ☒	E ☒	H ☐
Doç. Dr. Abdi SAĞCAN	Kardiyoloji	Kent Hastanesi	E ☒	K ☐	E ☐	H ☒	E ☐	H ☒
Doç. Dr. Korhan Barış BAYRAM	Fiziksel Tıp ve Rehabilitasyon	İKÇÜ ATATÜRK EAH	E ☒	K ☐	E ☐	H ☒	E ☒	H ☐

2/3

Appendix Figure B-2 The Second Page of The Ethical Approval Form

Appendix Figure B-3 The Last Page of The Ethical Approval Form

3/3

58